Quaternary Science Reviews 144 (2016) 107–122

Contents lists available at ScienceDirect

Quaternary Science Reviews

journal homepage: www.elsevier.com/locate/quascirev

Evidence for extreme floods in arid subtropical northwest Australia during the Little Ice Age chronozone (CE 1400–1850)

A. Rouillard [a, *], G. Skrzypek [a], C. Turney [b], S. Dogramaci [a, c], Q. Hua [d], A. Zawadzki [d], J. Reeves [e], P. Greenwood [a, f, g], A.J. O'Donnell [a], P.F. Grierson [a]

[a] Ecosystems Research Group and West Australian Biogeochemistry Centre, School of Plant Biology, The University of Western Australia, Crawley, WA 6009, Australia
[b] Climate Change Research Centre, School of Biological, Earth and Environmental Sciences, University of New South Wales, Sydney, NSW 2052, Australia
[c] Rio Tinto Iron Ore, Perth, WA 6000, Australia
[d] Australian Nuclear Science and Technology Organisation (ANSTO), Locked Bag 2001, Kirrawee DC, NSW 2232, Australia
[e] Faculty of Science and Technology, Federation University Australia, PO Box 663, Ballarat VIC 3353, Australia
[f] Centre for Exploration Targeting, School of Earth and Environment, The University of Western Australia, Crawley, WA, Australia
[g] Western Australia Organic and Isotope Geochemistry Centre, The Institute for Geoscience Research, Department of Chemistry, Curtin University, Bentley, WA, Australia

ARTICLE INFO

Article history:
Received 2 December 2015
Received in revised form
28 April 2016
Accepted 9 May 2016

Keywords:
Hydroclimate
Intertropical Convergence Zone (ITCZ)
Late Holocene
Little Ice Age (LIA)
Sediment
Paleolimnology
Pilbara

ABSTRACT

Here we report a ~2000-year sediment sequence from the Fortescue Marsh (*Martuyitha*) in the eastern Pilbara region, which we have used to investigate changing hydroclimatic conditions in the arid subtropics of northwest Australia. The Pilbara is located at the intersection of the tropical Indian and Pacific Oceans and its modern rainfall regime is strongly influenced by tropical cyclones, the Intertropical Convergence Zone (ITCZ) and the Indo-Pacific Warm Pool. We identified four distinct periods within the record. The most recent period (P1: CE ~1990–present) reveals hydroclimatic conditions over recent decades that are the most persistently wet of potentially the last ~2000 years. During the previous centuries (P2: ~CE 1600–1990), the Fortescue Marsh was overall drier but likely punctuated by a number of extreme floods, which are defined here as extraordinary, strongly episodic floods in drylands generated by rainfall events of high volume and intensity. The occurrence of extreme floods during this period, which encompasses the Little Ice Age (LIA; CE 1400–1850), is coherent with other southern tropical datasets along the ITCZ over the last 2000 years, suggesting synchronous hydroclimatic changes across the region. This extreme flood period was preceded by several hundred years (P3: ~CE 700–1600) of less vigorous but more regular flows. The earliest period of the sediment record (P4: ~CE 100–700) was the most arid, with sedimentary and preservation processes driven by prolonged drought. Our results highlight the importance of developing paleoclimate records from the tropical and sub-tropical arid zone, providing a long-term baseline of hydrological conditions in areas with limited historical observations.

1. Introduction

There is increasing interest in using climate fluctuations over the last ~2000 years to place recent multi-decadal trends in the context of long-term change, including exploring the relative role of natural versus anthropogenic factors as drivers of change (e.g., Masson-Delmotte et al., 2013; PAGES 2K Consortium, 2013). However, determining the direction of change in the hydroclimate has been challenging in regions where there is a relative paucity of records and high spatial and interannual variability in rainfall. The situation is particularly acute in the Southern Hemisphere

Abbreviations: CE, Common Era; CIC, Constant Initial Concentration; CRS, Constant Rate of Supply; ENSO, El Niño-Southern Oscillation; IASM, Indonesian Australian Summer Monsoon; IC, Inorganic Carbon; ITCZ, Intertropical Convergence Zone; LIA, Little Ice Age; MJO, Madden-Julian/Intra-seasonal Oscillation; NH, Northern Hemisphere; OC, Organic Carbon; OM, Organic Matter; SAM, Southern Annular Mode; SH, Southern Hemisphere; TC, Tropical Cyclone.

* Corresponding author. Present address: Centre for GeoGenetics, Natural History Museum of Denmark, University of Copenhagen, Øster Voldgade 5-7, 1350 Copenhagen K, Denmark.
E-mail addresses: alexandra.rouillard@snm.ku.dk, alexandra.rouillard@research.uwa.edu.au, alexandrarouillard@yahoo.ca (A. Rouillard).

http://dx.doi.org/10.1016/j.quascirev.2016.05.004
0277-3791/

(Neukom and Gergis, 2012; Palmer et al., 2015). Paleo-studies and synthetic analyses have nevertheless identified significant and largely coherent shifts in tropical and sub-tropical hydroclimates during the late Holocene across Africa (e.g., Verschuren, 2004; Verschuren and Charman, 2008; Tierney et al., 2013), Central and South America (Haug et al., 2001; Hodell et al., 2005; Bird et al., 2011; Cuna et al., 2014), the Pacific (Sachs et al., 2009) and globally (Graham et al., 2011). Although sub-regional variations in tropical hydroclimatic trends have been recognised (e.g., Stager et al., 2013; Burrough and Thomas, 2013; Woodborne et al., 2015), there is a remarkable global coherence in hydrologic shifts for some periods, suggesting changes in the Intertropical Convergence Zone (ITCZ) (driven by Northern Hemisphere latitudinal temperature gradients) and/or the El Niño Southern Oscillation (ENSO) may play a role (Sachs et al., 2009; Graham et al., 2011; Schneider et al., 2014).

Strikingly, one of the most consistent features of synchronous changes in the tropics is associated with the cooler temperatures of the Little Ice Age (LIA) in the Northern Hemisphere (NH), defined here as a chronozone between CE 1400 and 1850 (PAGES 2k Consortium, 2013). A NH summer cooling is thought to have caused a southward shift or poleward expansion in the ITCZ and associated tropical rain belt (Broccoli et al., 2006; Yancheva et al., 2007; Sachs et al., 2009; Mohtadi et al., 2014). It has thus been hypothesised that the northern and southern tropics and subtropics experienced antiphase shifts in hydrology during the LIA: with drier conditions in the north mirrored by wetter conditions in the south (e.g., Haug et al., 2001; Verschuren, 2004; Sachs et al., 2009; Cuna et al., 2014).

Recent reviews of the Quaternary records from the Australian tropics and interior arid zone, including marine sediments off the northwest coast that have been used to reconstruct relative aridity and monsoonal dynamics during glacial and interglacial periods (van der Kaars and De Deckker, 2002; van der Kaars et al., 2006; De Deckker et al., 2014; Stuut et al., 2014), surmise increasingly arid conditions during the late Holocene (Fitzsimmons et al., 2013; Reeves et al., 2013a, b). However, the resolution of these reconstructions is not sufficient to allow comparisons to more recent hydroclimatic variation (e.g., Proske et al., 2014). A recent synthesis based on Australasian records and modelling has proposed rainfall patterns over the Australasian tropics followed a different trajectory to other continents during the late Holocene (Yan et al., 2015). Unfortunately, the dearth of Australian terrestrial paleohydrological records with sufficient (sub-centennial) temporal resolution is extremely limited, preventing the testing of hypothesised asynchronous change in rainfall across the region and more broadly, the Southern Hemisphere (Neukom and Gergis, 2012). In northwest Australia, for example, rainfall delivery today is dominated by synoptic weather systems associated with the ITCZ, particularly tropical cyclones (TCs) and monsoon lows (McBride and Keenan, 1982; Berry et al., 2011; Lavender and Abbs, 2013; Ng et al., 2015). The few published reconstructions, however, have had limited success in extending the regional hydroclimate record. For instance, speleothem $\delta^{18}O$ records from the northwest coast spanning the last 1500 years have suggested the lowest level of cyclonic activity over this period to be since 1960, which is in marked contrast to the weak observed relationship between speleothem $\delta^{18}O$ and rainfall volume (Haig et al., 2014), observational trends (Shi et al., 2008; Taschetto and England, 2009; Gallant and Karoly, 2010) and inferences over the last 150 years from tree ring records from locations further inland (Cullen and Grierson, 2007; O'Donnell et al., 2015). These contradictory findings clearly demonstrate the urgent need for further reconstructions from terrestrial environments across the region.

In this study, we report a new sedimentary record of climate variability for the past ~2000 years from the Fortescue Marsh, eastern Pilbara (northwest Australia), a site known to capture regional hydroclimatic change resulting from flash surface flooding (Skrzypek et al., 2013; Rouillard et al., 2015). Our objectives were to (i) improve the temporal resolution and spatial coverage of late Holocene hydroclimatic variability in northwest Australia and (ii) elucidate shifts involved in hemispheric circulation dynamics and associated patterns of rainfall that may relate to the LIA chronozone.

2. Methods

2.1. Regional settings and site description

The eastern Pilbara is located approximately 400 km inland of the northwest Australian coast (22°S 119°E; Fig. 1). The seasonal variability in rainfall is summer-dominated (Fig. 2), and interannual variability is one of the most extreme in the world (van Etten, 2009). The majority of rainfall is delivered over 1–5 days events by TCs and other closed lows. In contrast with South American and continental and west African Southern Hemisphere (SH) subtropics, the contribution of TCs to annual rainfall in the eastern Pilbara (30–40%) is one of the highest globally (Dare et al., 2012; Lavender and Abbs, 2013; Ng et al., 2015). Evaporation rates in the catchment (~2800–3200 mm yr^{-1}) are up to ten-fold higher than the average annual rainfall of ~290 mm (www.bom.gov.au/climate/data/).

The Fortescue Marsh (hereafter referred to as the Marsh and known as *Martuyitha* to indigenous peoples) lies in the Fortescue Paleovalley, which is flanked by the Chichester and Hamersley ranges. The Marsh acts as a terminal basin for the Upper Fortescue River catchment (30,000 km^2; Fig. 1a). The Upper Fortescue River catchment, including the Marsh, is not hydrologically connected to the Lower Fortescue River catchment (Skrzypek et al., 2013). The Fortescue River drains 56% of the Upper Fortescue River catchment where it reaches the Marsh (Fig. 1a). Gauging stations in the catchment are limited; however, a continental-scale classification of stream and river flow regime based on <20 years of discharge records in the region described flow as being 'variable summer extremely intermittent' (Kennard et al., 2010). This flow regime class is the most extreme on the Australian continent and is described by the highest number of zero flow days (>250 per year), lowest baseflow index, highest variability and skewness of daily flows, and in the timing of maximum flows, highest rise and fall rate (up to ~20 and 5 ML day^{-1}, respectively). This extreme regime has however predictable high flows (>1st percentile) with daily volumes in excess of 15 ML day^{-1}.

We extracted sediment cores from 14 Mile Pool, a relatively large pool located on the eastern boundary of the Fortescue Marsh (Fig. 1). The generally shallow (<2 m) pool represents a terminal reach (~2 km long) of the Upper Fortescue River at the head of the Marsh (Fig. 1a). 14 Mile Pool is the most frequently inundated and perennial water feature of the Marsh and receives most of the flow that subsequently progresses west across the floodplain (Rouillard et al., 2015). The hydraulic gradient along the Upper Fortescue River between Newman and 14 Mile Pool is 0.0007. To the north, 14 Mile Pool drains a section of the Chichester Ranges (hydraulic gradient of 0.006, and 0.003 over the immediate 15 km), which represents only 3% of the pool's total catchment area. 14 Mile Pool was selected after an extensive coring survey across the Marsh and along the major creek lines upstream in the Upper Fortescue River system; at other sites surveyed, sediment sequences were either mixed vertically (fine particles, silty clays in claypans on the floodplain) or clearly scoured by high energy flash floods (i.e., coarser particles, sandy and gravelly beds of pools higher up in the ranges).

The bed of the pool at the coring location is ~75 m wide

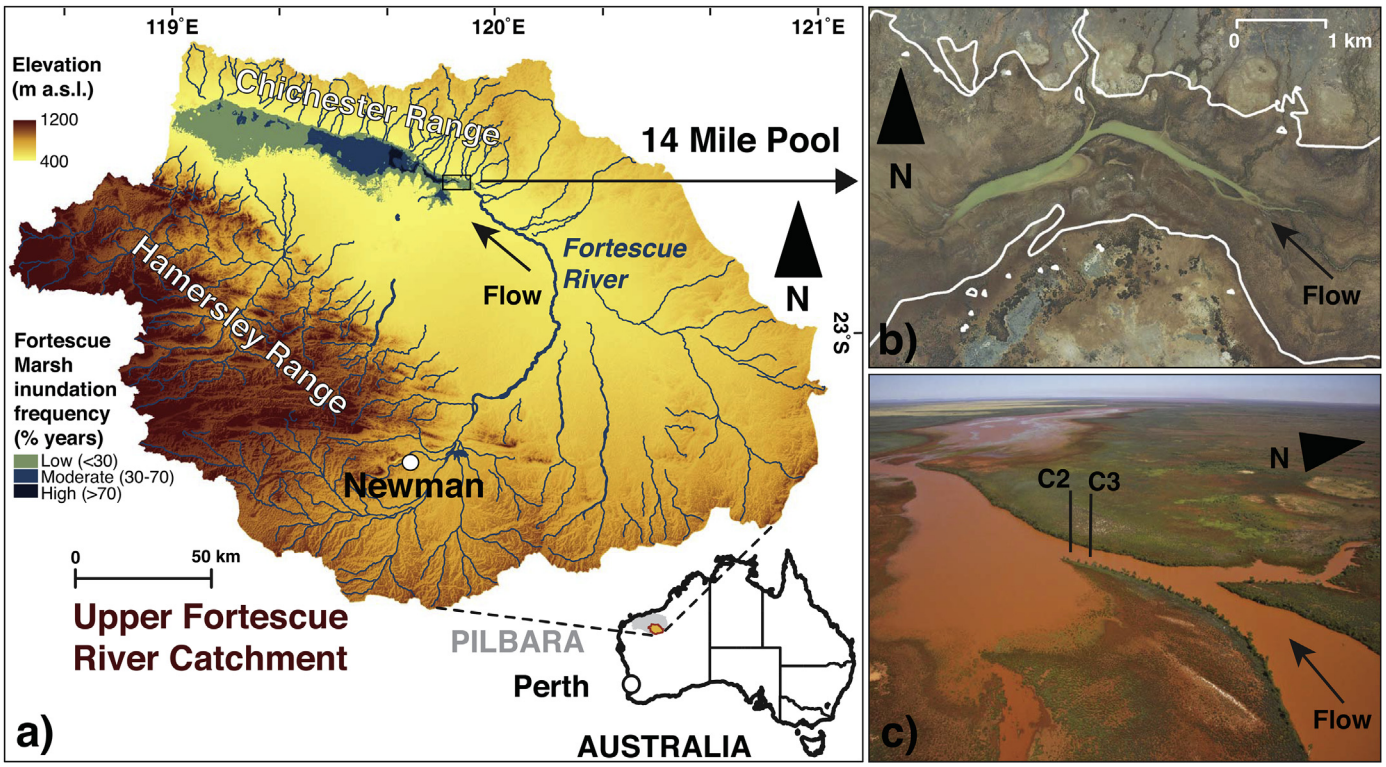

Fig. 1. **a)** Topographic (1 Sec. SRTM Derived DEM-H v.1; Geoscience Australia) and (intermittent) river network (Geoscience Australia) map of the Fortescue Marsh catchment (i.e., Upper Fortescue River catchment), including the present study site (14 Mile Pool), and frequency of inundation of the Marsh (modified from Rouillard et al., 2015); **b)** 40 cm resolution ortho-photo (July 2010; Fortescue Metals Group Ltd) overlaid by maximum 1988–2014 floodplain (solid white line; Rouillard et al., 2015); **c)** aerial photograph taken on Feb 2012 (A. Rouillard) showing the coring location of replicate cores FOR106C2 (C3) and FOR106C3 (C3).

(~405.5–406 m a.s.l.) and overflows on to a 1400 m wide floodplain (407–407.5 m a.s.l.) during short-lived flooding events (Fig. 1b). The inundation regime at the Marsh over the last 100 years has been strongly dominated by TC-generated, high-volume summer rainfall events resulting in flash floods (Rouillard et al., 2015). Between 1988 and 2012, surface water on the 14 Mile Pool and floodplain typically receded to the pool's bed and became isolated from the Upper Fortescue River within a month of flooding, but on average remained connected to the other downstream sections of the Marsh for 3–4 months every year. During large wet years (>300 km^2 inundations), which occurred about once in 10 years over the last century, downstream connectivity of 14 Mile Pool with the Marsh persisted for up to 10 months (Rouillard et al., 2015).

Water chemistry measurements taken between 2010 and 2012, including quantification of evaporative loss using water stable isotopes and ionic concentration of salts, show that 14 Mile Pool experiences large shifts in volume (i.e., affecting depth, width and length) in response to flooding and seasonal or prolonged supra-seasonal drying rather than being sustained by groundwater (Skrzypek et al., 2013). Fresh, slightly acidic, softwater and nutrient poor conditions brought by flooding progressively develop into brackish (total dissolved solids = 60–6000 mg L^{-1}), alkaline (pH = 6.6–9.9), hardwater (HCO_3^- = 23–308 mg L^{-1}) and slightly enriched in nutrients (total filterable phosphorus = <0.01–0.2 mg L^{-1}; total filterable nitrogen = 0.4–4 mg L^{-1}) over time as water evaporates. Daytime water temperature varies between 13 and 36 °C. Turbidity of the pool is at its highest within the month following flooding (10–240 NTU), and during the dry winter season when the pool is most shallow. However, the water column clears very quickly once flooding subsides as clays settle to the bottom of the pool enabling algal and macrophytic growth.

14 Mile Pool is flanked by a narrow band of riparian vegetation on both banks dominated by large *Eucalyptus camaldulensis* and *Eucalyptus victrix* trees (Fig. 1c). Beyond the riparian corridor, salt-, drought- and inundation-tolerant succulents (*Tecticornia* and other chenopods) dominate the floodplain vegetation (Beard, 1975). Early cadastral maps (Fig. A.1; Dept of Lands and Surveys, 1892, 1894, 1899, 1905a,b, 1909, 1919, 1921, 1924, 1952), aerial photographs (1957; Edward de Courcy Clarke Earth Science Museum, UWA) and high-resolution ortho-rectified imagery (2004, 2006, 2010, 2012 and 2013; www.landgate.wa.gov.au) indicate that there has been no major change in the site location (1892) and morphology (1905) of 14 Mile Pool since at least this period (i.e., coverage of the earliest cadastral map available for the area showing the position of a watering point at current location; Fig. A.1).

2.2. Core collection and processing

Two 0.6 m replicate sediment cores (codes FOR106C2 & FOR106C3; 22°33′20.4″S 119°51′40.9″E & 22°33′19.2″S 119°51′42.3″E, respectively) were extracted 50 m apart below 1.8 m of water (bank full) in November 2011 from the deepest section of 14 Mile Pool (Fig. 1c) using a modified percussion corer activated from a floating platform. To select the coring location, we surveyed satellite imagery over the 1988–2012 period (Rouillard et al., 2015) to observe seasonal drying sequences of the 14 Mile Pool and to determine the most frequently and most persistent inundated section of the pool. Briefly, all the captured imagery from the *Landsat* archive over our study site was compiled and analysed, with episodic coverage between 1972 and 1988 and nearly fort-nightly resolution between 1988 and 2012 (see Rouillard et al., 2015 for further details). We also conducted seasonal field surveys over

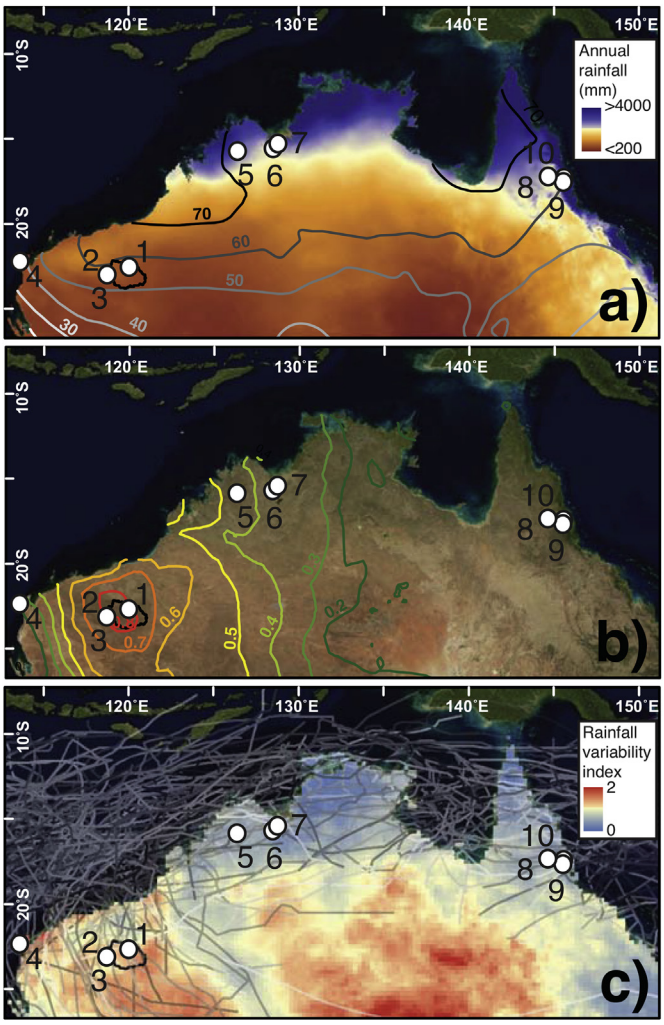

Fig. 2. a) Annual rainfall (shading), percentage of average annual rainfall that falls in Jan–Mar (isohyets; www.bom.gov.au) and locations of published terrestrial paleohydrological records in tropical and subtropical Australia with sub-centennial resolution discussed in the text, including (1) Fortescue Marsh, present study; (2) Juna Downs (Cullen and Grierson, 2007); (3) Hamersley Range (O'Donnell et al., 2015); (4) Cape Range and (8) Chillagoe (Haig et al., 2014); (5) Black Springs (McGowan et al., 2012); (6) KNI-51 (Denniston et al., 2013, 2015); (7) King River (Proske et al., 2014); (9) Bromfield Swamp and (10) Mount Quincan (Burrows et al., 2014); overlaid on Upper Fortescue River catchment (black line); **b)** April true colour MODIS composite image (Blue Marble Next Generation with Topography; www.visibleearth.nasa.gov/view.php?id=74318) and isohyets of the correlation strength (r) between summer rainfall and Hamersley Range tree-ring growth (modified from O'Donnell et al., 2015), and **c)** interannual variability in rainfall (www.bom.gov.au) and 1979–2012 TCs tracks (Tropical Cyclones Database; www.bom.gov.au/cyclone).

the 2009–2012 period, which confirmed large variation in water volume of the pool (i.e., depth, width and length) in response to flooding and seasonal or prolonged supraseasonal drying and that only the location chosen for coring remained inundated. Bathymetric assessment confirmed that cores were obtained from the deepest section of the 14 Mile Pool (Sep. 2011). We also conducted a second coring survey in November 2012 in the same section of the pool (at the location of FOR106C3), where two percussion cores (to compacted base layer; ~60 cm) and two hand pushed cores (~20 cm) were taken from the floating platform in only 50 cm water depth. These cores confirmed a coherent longitudinal lithology in the section that was consistent after a major flood event. In summer 2012, TC Heidi (Jan 11–13) generated up to 184 mm of rain overnight in the Upper Fortescue catchment that we estimated, based on data collected from newly installed piezometers across the Marsh, resulted in >400 GL of water to the Marsh. However, the sequences extracted before (Nov 2011) and after this large flood (Nov 2012) had the same apparent lithology, including distinct, sub-cm horizontal layering in the top 5 cm of the core.

Despite multiple coring attempts, longer sediment profiles could not be retrieved due to an underlying cemented layer. The 5-cm diameter cores were split lengthwise in the lab using a rotating saw and stainless steel wire, and the texture, layering and colour of the split cores were characterised visually. One half was wrapped in plastic and aluminium foil and preserved at 4 °C as a reference. The other half was sub-sectioned in 1 cm thin slices. Subsamples from the centre portion (diameter ~ 3 cm) that had not been in direct contact with the PVC piping were placed in aluminium foil and used for dating and isotope analyses, while the outer portion of the 1 cm sections were bagged and used for microfossil and granulometric analyses. All discrete intervals were frozen at −20 °C directly prior to freeze-drying for measurement of moisture content. Mineralogy was established using X-ray diffraction (XRD) on random powder using a Philips PW3020 diffractometer at depths 8, 46 and 57 cm (FOR106C3).

2.2.1. Particle size analysis

Particle characterisation was made on FOR106C3 using a series of phi stainless steel sieves. Prior to sieving through a 1 mm mesh sieve, the sediment was screened for macrofossils and the >1 mm fraction analysed for particle size. An aliquot (~0.5 cm^3) of the <1 mm fraction was analysed in Calgon ($Na_6O_{18}P_6$) using a Malvern Mastersizer 2000 with Hydro2000G light scattering laser counter. Measurements were made in triplicate and average values were used to build a frequency histogram. GRADISTAT v.4.0 software (Blott and Pye, 2001) was used to calculate the statistical grain size parameters (mean, median, sorting/standard deviation, sand, silt, clay and gravel percentages) on the integrated >1 mm and <1 mm fractions using the method of moments with geometric scaling.

2.2.2. Total C and N and stable isotopic signatures

Total C and N (%) contents and stable isotope signatures ($\delta^{13}C$ and $\delta^{15}N$) of the <1 mm fraction of every 1 cm interval (FOR106C3) were obtained using a Thermo Flush Elemental Analyser coupled with a Delta V Plus Isotope Ratio Mass Spectrometer (Thermo Fisher Scientific, Bremen, Germany) at the West Australian Biogeochemistry Centre at The University of Western Australia (www.wabc.uwa.edu.au). All samples were freeze-dried, ground and homogenized prior to analyses. Sediment organic carbon (OC) content and $\delta^{13}C$ were also determined for every other interval of the 60-cm long profile (FOR106C3). Following standard protocols, app. 100–150 mg was pre-treated at room temperature overnight with acid (4% HCl) to remove carbonates (Brodie et al., 2011). However, acid pre-treatment for the removal of inorganic carbon (IC) commonly introduces biases in $\delta^{13}C$ and C estimates beyond instrumental precision (e.g., 4‰; Brodie et al., 2011). Given the very low total C content of our samples and the low variability they showed in $\delta^{13}C$ (generally <1‰), the removal of IC for determination of bulk OC content and $\delta^{13}C$ values was considered unreliable. Thus, we report our findings as non-acidified. All stable isotope analyses have been reported in permil (‰) after multi-point normalisation to international scales using NBS19, USGS24, NBS22, LSVEC for $\delta^{13}C$ and IAEA-N1, IAEA-N2, USGS32 for $\delta^{15}N$ (Skrzypek, 2013), with combined analytical uncertainty of <0.10‰. Correction of total content of C and N was applied to account for the proportion of the weight of the <1 mm fraction.

2.2.3. Subfossil analysis

Where present, ostracod shells were systematically sampled from the full core for every 1-cm interval of the loose freeze-dried sediment for identification (FOR106C3). The extensive iron oxide coating was individually removed from the shells in a sonication bath of deionised water (10 s). After a coarse resolution (10-cm) analysis for microfossils, pollen of *Chenopodiaceae*, *Poaceae*, *Myrtaceae* and *Asteraceae* families were identified. Overall pollen concentrations were found to be very low (averaging ~5000 grains cm^{-3}; Shulmeister, 1992), however, and no pollen was found in the basal samples. Preservation rates were also very low, with <20% non-deteriorated grains per interval in the majority of cases. Deteriorated grains were primarily crumpled, most likely reflecting mechanical damage resulting from compaction, inwash or sediment disturbance through, for example, rewetting and subsequent drying of the sediment cracking clays (Cushing, 1967; Lowe, 1982), which also corresponded with the results of preliminary diatom analysis. Given the low concentrations coupled with high levels of deterioration evident in the sequence, it was determined likely that the non-deteriorated microfossils would represent types more resistant to decay, rather than past assemblages per se.

2.3. Developing a chronological framework

A geochronological framework for the sequence was established using ^{210}Pb, ^{137}Cs and accelerator mass spectrometry (AMS) ^{14}C radioisotopic techniques (Appleby, 2001; Björck and Wohlfarth, 2001). ^{210}Pb and ^{137}Cs activities were measured on ~2 cm^3 freeze-dried sediment from 18 intervals of replicate core FOR106C3 using gamma counters at the Paleoecological Environmental Assessment and Research Laboratory (PEARL, Queen's University, Kingston, Ontario, Canada) following Schelske et al. (1994). AMS ^{14}C dating was performed at the STAR facility at the Australian Nuclear Science and Technology Organisation (ANSTO) at Lucas Heights, NSW Australia (Hua et al., 2001; Fink et al., 2004) and Waikato Radiocarbon Dating Laboratory (Hamilton, New Zealand). Given the consistent lithologies between replicate cores FOR106C2 & FOR106C3, eight terrestrial plant macrofossils (fresh and charred) and six bulk samples were extracted from both cores for AMS ^{14}C analysis: depths from FOR106C2 were converted to FOR106C3 depths by linear interpolation between distinct lithological sections. Radiocarbon ages were calibrated to Common Era (CE) years using atmospheric bomb ^{14}C data for the Southern Hemisphere (SH) Zone 1–2 (Hua et al., 2013) and extended back in time by the SHCal13 calibration curve (Hogg et al., 2013) and OxCal v. 4.2 program (Bronk Ramsey, 2009). Unless explicitly described otherwise, ages mentioned henceforth are quoted in CE years.

3. Results

3.1. Age-depth models

The three dating techniques employed (^{210}Pb, ^{137}Cs and ^{14}C) provided coherent chronologies for the sequence. As might be expected for such arid and extreme hydrologic conditions, sedimentation rates were not linear and the sequence is likely discontinuous (Figs. 3 and 4). ^{210}Pb and ^{137}Cs activity concentrations, used for the most recent history of the sequence, were both low (values below 100 and 5 Bq kg^{-1}, respectively) but comparable to other lacustrine sediments from the SH (Gell et al., 2005; Leslie and Hancock, 2008). Total ^{210}Pb activity for the 13 samples analysed generally declined with depth but several inversions from this trend were also evident (Fig. 4a). Below 40 cm depth the unsupported ^{210}Pb activities were too low to be used in the dating calculations, whereby total ^{210}Pb activities were not significantly different from supported ^{210}Pb activities, estimated (i.e., averaged) to be ~30 Bq kg^{-1}. In the top 40 cm of the core, the lower unsupported ^{210}Pb activities ('low activities' sample series; Fig. 4a), were not used either as these activities may represent older sediment materials from the catchment being re-deposited over more recent materials during large floods ('dilution effect'; Appleby, 2001) or some level of re-suspension and mixing at the sediment-water interface. This interpretation of the irregular depositional pattern is supported by the lithological layering, where we observed an abrupt horizontal colour and grain size change in this section of the core (Fig. 3). Additional variability in the supported ^{210}Pb activities (background) can also be seen from the uneven ^{214}Bi profile (Fig. 4a). Thus, only the five top samples (8–33 cm) with higher unsupported activities ('high activities' sample series; Fig. 4a, b) representing 'non-flood related depositions' were used in the chronology reconstruction.

Based on these five selected samples, the Constant Initial Concentration (CIC) and Constant Rate of Supply (CRS) models provided close agreement on ^{210}Pb age determinations (i.e., within analytical uncertainties); the CRS was ultimately selected as it was better suited to the variable accumulation rate of this core (Appleby, 2001). For verification of sample selection in the top 40 cm of the core, we also calculated age estimates from the discarded 'low activities' samples as an independent series but found no difference in estimates between series (Fig. 4a). The highest ^{137}Cs activities were measured between 16.5 and 19.5 cm, delineating a depth range for the peak nuclear testing of 1964 in the SH (Fig. 4c) and supporting the calculated CRS model ^{210}Pb chronology (Leslie and Hancock, 2008). The onset of ^{137}Cs was identified at 28–29 cm, which should correspond to the early detection of ^{137}Cs fallout from nuclear testing (CE, 1954–1957) (Leslie and Hancock, 2008).

Two age-depth models were constructed for the sequence (Fig. 3). The surface was assigned as CE 2012 as the date of coring as it immediately followed a major flood event (Rouillard et al., 2015). The first age-depth model (Model 1) was based on the eight radiocarbon dates of terrestrial macrofossils (Fig. 3; Table A.1 and A.2). Bulk samples yielded older ^{14}C ages compared to those of terrestrial macrofossils at the same depths, possibly reflecting a hard water effect as a result of carbonate bedrock (Björk and Wohlfarth, 2001) and/or transportation of older (reworked) material from the catchment. However, the offset that could be attributed to the reservoir effect was not constant through time, ranging from 240 to 2483 yr (Table A.1). Considering the high level of biological reworking of organic material that takes place in arid environments, it is likely that the bulk-dated organic compounds were highly recalcitrant terrestrial compounds transported from the surrounding catchment during flooding and/or preferentially preserved with depth mixed with a variable amount of organic matter (OM) produced in situ (Battin et al., 2008). Thus, bulk samples were not used for the age-depth models (Table A.1 and A.2).

We used two approaches to estimate the age of the sediments from 14 Mile Pool. Model 1 was built using the Bayesian P_Sequence model in the OxCal program v. 4.2 (Bronk Ramsey, 2009) with a low k value of 0.7 to allow flexibility in the model (Fig. 3). The overall agreement index of the model was 59%, which is very close to the accepted level of 60% (Bronk Ramsey, 2008). The second age-depth model (Model 2), which includes ^{14}C (8), CRS ^{210}Pb (5) and ^{137}Cs (2) age estimates, was performed in CLAM (Blaauw, 2010) using smooth spline fitting with a goodness-of-fit of 15.11 (Fig. 3). The main differences in the outputs of the models are

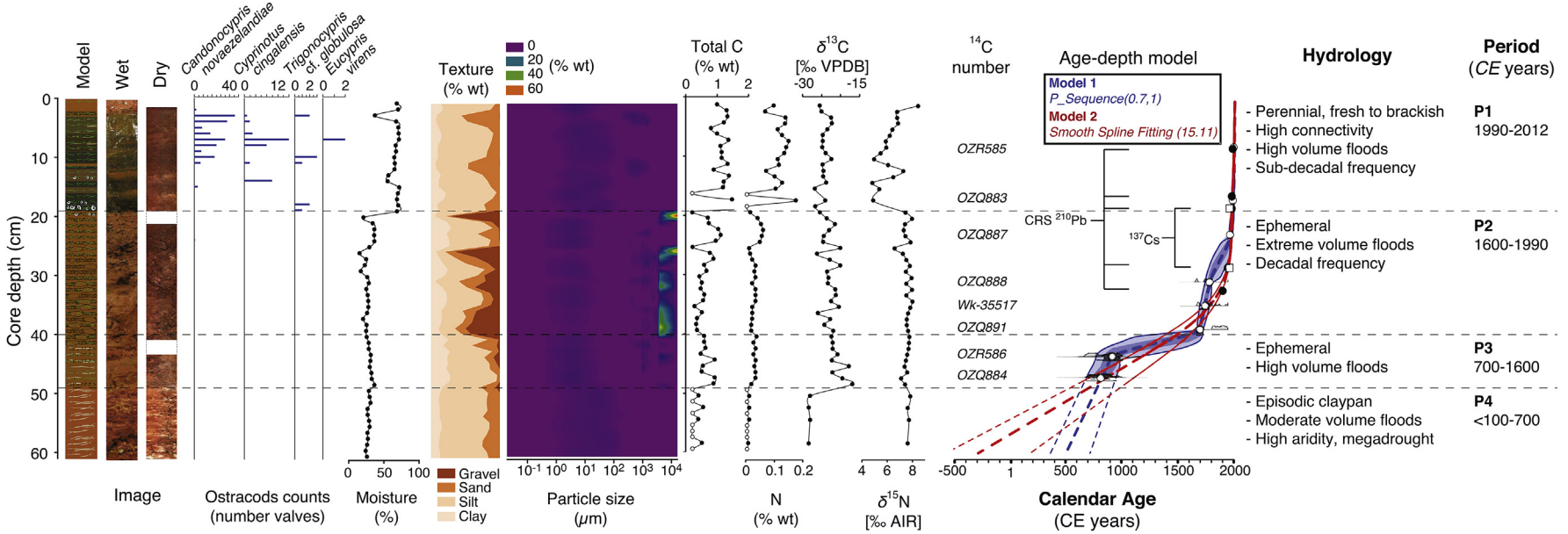

Fig. 3. Stratigraphy of 14 Mile Pool core. From left to right: schematic representation (Model); high-resolution photographs (Wet and Dry); number of ostracod valves; moisture content (% weight); statistical grain-size parameters (gravel, sand, silt and clay fractions; % volume < 1 mm; % weight > 1 mm) (GRADISTAT 4.0; Blott and Pye, 2001); grain size 3D surface plots (z axis = % volume < 1 mm; % weight > 1 mm); total C and N content (% weight); bulk $\delta^{13}C$ [‰ VPDB] and $\delta^{15}N$ [‰ AIR], laboratory codes for AMS ^{14}C age estimates (^{14}C number); age-depth Bayesian P_Sequence Model 1 rived from ^{14}C ages only (blue series; OxCal v. 4.2; Bronk Ramsey, 2009) and Smooth Spline Fitting Model 2 based on all ages including ^{210}Pb, ^{137}Cs and ^{14}C (red series; CLAM; Blaauw, 2010), with respective 95% confidence intervals envelopes and model extrapolations (<48 cm depth), ^{14}C age estimates (open circles) and their probability distributions (2σ envelope in grey; OxCal v. 4.2), Constant Rate of Supply (CRS) ^{210}Pb (closed circles) and ^{137}Cs (squares) age estimates; hydrological interpretation; and time period (transitions estimated from the average values provided by Models 1 & 2 in the adjoining intervals).

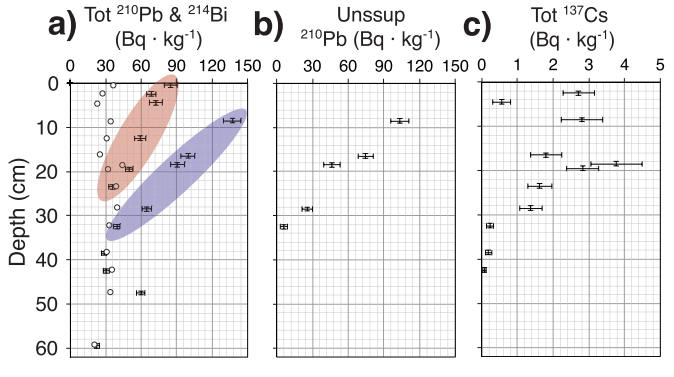

Fig. 4. Gamma counting results from 14 Mile core (FOR106C3), including **a)** total ^{210}Pb (with error bars) of all analysed intervals, including the selected 'high activities' (blue shading) and discarded 'low activities' (red shading) sample series for the age calculations and ^{214}Bi activity (i.e., a proxy for supported ^{210}Pb; open circles); **b)** unsupported ^{210}Pb activity (with error bars) included in age-depth Model 2 (see Sect. 3.1 for details of selection); and **c)** total ^{137}Cs (with error bars). (For interpretation of the references to colour in this figure legend, the reader is referred to the web version of this article.)

in the age estimation of the P3–P2 boundary and the early onset of the profile; Model 1 places these boundaries at ~150 and 800 years later than Model 2, respectively. Given the sequential but likely discontinuous depositional patterns of the system (intermittent sedimentation and transport) and the effect of sub-aerial drying on the sequence (weathering, wind deflation), these age-depth models have been applied here to provide age estimates of the boundaries for key hydrologic periods (described here as P1–4) and sedimentation rates (averaging between models). More detailed implications of sequence discontinuities and the differential between models on boundary estimates for paleohydrological interpretations are discussed below for each period.

3.2. Multi-proxy paleohydrological reconstruction

All age-depth models identified several inflections in sedimentation (Fig. 3). Four stratigraphic units (P1–4) were identified from shifts in sediment accumulation rates and other sediment properties (i.e., particle size distribution, moisture content, oxidation state, macrofossil abundance and C and N content and stable isotopes) (Fig. 3), which most probably indicate different hydrological conditions in the four periods. These different hydrological regimes may either reflect the catchment hydroclimatic history, shifts in catchment processes affecting runoff and erosional patterns from land use (post 1860s) or a morphological shift in the river channel position through lateral displacement or an avulsion event (Jones and Schumm, 2009). Avulsion events (when the old river channel is abandoned and a new river channel is formed) are well documented elsewhere on low gradient floodplains in the arid zone (e.g., Ralph et al., 2011; Donselaar et al., 2013). However, they are unlikely at 14 Mile Pool given the local geomorphological conditions described above (topography, soil type, stability of long-lived vegetation on banks) and the consistency in the observed mineralogical profile (Figs. 1 and 4). The mineralogy of the sequence was dominated by alumina-silicate clays ('cracking clays') with a smaller proportion of iron oxides and consistent with depth (i.e., the mineralogy was almost always mainly kaolinite and quartz with moderate amounts of illite (hydromuscovite), goethite, and hematite). The strong relationship between rainfall variables and surface water hydrology at the Marsh over at least the last 30 years also suggests these processes would have a relatively low influence on runoff in comparison to the hydroclimate (Rouillard et al., 2015).

3.2.1. Stratigraphic changes over the last 2000 years

3.2.1.1. Period 1 (P1)—CE 1990 to present: a perennial water hole in the desert. The uppermost sediments (<19 cm) clearly capture a relatively fast (i.e., the highest in the record), sequential but irregular aggradation of alluvial sediment (0.3–0.6 g cm^{-2} yr^{-1}) in a perennial, aquatic environment, encompassing the last ~20 years (average age of 18–20 cm transition from models 1 and 2 = 1991). The dilution pattern identified from the ^{210}Pb chronology (Appleby, 2001) suggests high-energy flooding of the pool contributed transported sediment from the upstream floodplain to the sequence (Fig. 4). The anoxic muds (inferred from the oxidation of the sediment once in contact with air), relatively high moisture content (>50%), abundance of well-preserved ostracods and presence of plant and other macrofossils combined with smaller grain size (<1 mm) and relatively high nitrogen content (mean = 0.12% dry wt; range = 0.06–0.17%) all suggest that 14 Mile Pool received regular inflows of water of small to high energy during this period (Fig. 3). A sedimentary water content of ~70%, however, is rather low for recent subaqueous lacustrine deposits but not unexpected considering the very low organic content (Verschuren, 1999; Bessems et al., 2008).

The slight depletion on average in both δ^{15}N (−1.4‰) and δ^{13}C (−1.3‰) in this period compared to the remainder of the profile further indicates a change in biogeochemical processes in this period. The low total C content detected in the Fortescue Marsh sediments (<1%) was similar to modern Pilbara soils and typical of sediment of dry stream beds (Ford et al., 2007; McIntyre et al., 2009a, b; Siebers et al., in press). Lower δ^{13}C values of the bulk sediment (−24.4‰) compared to the remainder of the core (−23.0‰) as well as higher C content for this record (mean = 1.4%; range = 0.8–5.6% wt; Fig. 3) suggest a relatively higher organic input (or lesser inorganic input, i.e., carbonates) compared to the typically more enriched carbonates (Finlay and Kendall, 2008). Alternatively, this change may reflect a lower input of OM with more positive δ^{13}C signatures such as C_4 grasses (−6 to −23‰) as opposed to C_3 plants (−23 to −34‰) (Schidlowski, 1987). Higher organic content in the sediment is consistent with relatively wetter conditions, where autochthonous primary production increases as a result of more frequent prolonged clear and fresh water phases (Coianiz et al., 2015). Wetter conditions may also result in: (i) increased production and transport of terrestrial OM from the catchment to the site through increased runoff (Battin et al., 2008); (ii) better preservation of OM under persistent anoxic conditions and limited sub-aerial oxidation of the clay-rich sediment (Verschuren, 1999); or (iii) a combination of these mechanisms. Bulk δ^{15}N data should always be interpreted along with other evidence as sediment sequences are complex and may be influenced by diagenesis and anthropogenic depositions (Brahney et al., 2014). Consequently, the lower δ^{15}N values in this context may reflect (i) the fixation of atmospheric N_2 by cyanobacteria or (ii) diagenetic microbial processing of in the sediment that would be favoured under perennial conditions (Brenner et al., 1999; Gälman et al., 2009).

Ostracods were only recovered from the top 19 cm of the core (with single valve found at 24 cm), corresponding to the period of ~1990–2012 (P1, Fig. 3). This high level of preservation in P1 also suggests limited drying during this period. Though the clay-rich sediment form a relatively impermeable streambed, prolonged drying would have caused any valves that may have been deposited

previously to be gradually dissolved by slightly acidic rainwater occasionally percolating through the dry sediment. The two dominant ostracod species identified (*Candonocypris novaezelandiae*, Baird, 1843; *Cyprinotus kimberleyensis*, Karanovic, 2008) in the top 15 cm of this period (Fig. 3) are freshwater species. The presence of male specimens of *C. novaezelandiae* in particular indicate more permanently inundated conditions because male offspring are only produced in favourable conditions (Radke et al., 2003). The presence of the resting stages of Cladocerans (i.e., epphippia) also suggests limited seasonal drying as these are micro-crustaceans that are generally absent in systems where droughts longer than 6–20 years occur (Jenkins and Boulton, 2003). This finding suggests that either annual summer inundations were large enough to maintain the aquatic habitat until the next rain season through significant recharge of the shallow river alluvium, or smaller pulses throughout the year contributed to the persistence of the surface water. The inundation extent at the Marsh over the last century (Rouillard et al., 2015) suggests a combination of both of these recharge patterns contributed to maintain the aquatic habitat. The coherent age-depth profile of P1 (Fig. 3) further indicates that any of the extreme flood events over the last ~20 years (Rouillard et al., 2015) were of insufficient energy to scour the sediment down to the bed of the pool. The onset of P1, however, may have been abrupt, as indicated by the presence of several land snail shells at the transition (18–20 cm) that were also found along the flood margins of the Marsh floodplain following the large inundation related to TC Heidi (Jan 2012).

3.2.1.2. Period 2 (P2)—CE 1600–1990: extreme floods. Period 2 (CE ~1600–1990; 19–40 cm; Fig. 3) is most remarkable due to an abrupt and major change in sedimentology that reflects a much higher energy environment and likely more variable hydrology than P1, P3 or P4. This period (P2) is characterised by a heterogeneous particle size matrix as well as the coarsest material in this record, i.e., fine to coarse (up to 2 cm) pebbles (Fig. 3). Virtually no microfauna were preserved in the sediments of this period. Total C (mean = 0.6% wt; range = 0.2–1.1% wt) and N (mean = 0.03% wt; range = 0.01–0.06% wt), while less than in P1, were also higher than either P3 or P4. Extreme flooding (i.e., much higher energy than P1) would have been necessary to carry the coarser bed load materials during this period, especially since the site is on a low gradient that should cause the erosion threshold to be relatively high (Powell, 2009). Coeval ^{14}C age determinations for the oldest part of this period (Table A.1) as well as the lower sedimentation rate for P2 (0.07–0.1 g cm^{-2} yr^{-1}) compared to P1 further suggest that extreme flooding might have occurred within a narrow time window as opposed to over the entire period, each event causing some degree of scour-induced hiatus(es) and mixing of the sediment (Fig. 3). Scouring of the sequence, specifically of the most recent portion of P3, which could also explain the apparent abrupt in sedimentation rate between P2 and P3 (Fig. 3). Sedimentary water content as low as 30–40% (Fig. 3) can only be explained by one or more episodes of prolonged drying (i.e., greater than current period) during the deposition of units P4-P2. Sub-aerial oxidation during those dry episodes explains, at least in part, the extremely low total C and N (Fig. 3; Verschuren, 1999), although both C and N contents in soils of the surrounding catchments are also invariably very low (Ford et al., 2007).

Given the low hydraulic gradient (i.e., 0.0007 over 100 km along the Upper Fortescue River to the east and, of lesser significance, 0.006 over 30 km to the north) of the pool's upstream floodplain and because relatively higher volume and/or more intense events would have been necessary to generate the shift in sedimentary patterns (i.e., pebble-sized particles, scouring) observed in P2 compared to the other periods of this record including documented very intense and high volume floods in the last 100 years, we describe these flooding events as 'extreme floods'. System memory or water storage has also been shown to significantly influence runoff and wetland inundations at the interannual level in arid environments worldwide (Reaney, 2008; Shook and Pomeroy, 2011). Here, the high energy floods during P2 would be consistent with more severe and/or intense rainfall events that likely followed prolonged periods of drought and resulted in supraseasonal-inundated conditions on the Marsh (Rouillard et al., 2015). In arid landscapes where soils are dominated by relatively impermeable clays, drought conditions cause vegetation cover to become sparser and can increase overland flow and flash runoff response (Sutfin et al., 2014). This interpretation would explain why the more perennial conditions of the pool during this period did not enable major scouring to occur, despite the multiple documented severe inundation events post-1990 at the Marsh (Rouillard et al., 2015). Owing to the large size of the material transported and deposited in to the 14 Mile Pool, we hypothesise that the size of these flood events in P2 were also likely larger than any observed over at least the last two decades (Rouillard et al., 2015; Fig. 3). We suggest the more intense floods captured by our multiproxy analysis in P2 compared to the remainder of the profile were caused by one or more episodic heavier and short-lived rainfall events, within an overall background of drier conditions.

The Pilbara has undergone relatively little change in catchment land use until the advent of mining in the region in the 1960s. Nevertheless, localised cattle and sheep grazing and the introduction of invasive grass species, as well as shifts in burning practices, might have influenced sedimentation rates of the 14 Mile Pool over the past century, as has been extensively documented elsewhere in the arid zone (e.g., Adair and Burke, 2010; Dunne et al., 2011; Eldridge et al., 2012). For example, pastoral use of 14 Mile Pool as a water point for sheep and cattle started in the late 1870s (Western Mail, 1917), and a stocking route went along the Fortescue River on the floodplain ~20 km upstream of the Pool (Fig. A.1). Stocking numbers peaked around the 1930s in the area (www.trove.nla.gov.au; McKenzie et al., 2009). Increased erosion along floodways was also reported in the Pilbara along with changes in vegetation in the early 1920s (McKenzie et al., 2009). Similarly, the invasive grass *Cenchrus ciliaris* was well-established in some areas of the catchment by the 1960s. However, the significant shift in sedimentation history recorded in the core at 14 Mile Pool does not occur until several decades after the most intensive pastoral disturbances (Fig. A.1 and 3).

3.2.1.3. Period 3 (P3)— CE 700–1600: lower interannual variability. Accumulation rates in this period (49–61 cm; Fig. 3) were likely at least ten-fold slower than P2 (i.e., 0.01 vs 0.07–0.1 g cm^{-2} yr^{-1}). When considered together with a finer particle size (<2 mm), these findings suggest 14 Mile Pool experienced flood events with relatively low to moderate energy that provided an ephemeral but relatively reliable seasonal hydrology between CE 700–1600 (P3, Fig. 3). $\delta^{13}C$ of total C was on average higher in P3 (+2.3‰) than in P2 although C and N contents were not significantly different than from those of P2 (Fig. 3). The inclusion of terrestrial plant and aquatic invertebrate (e.g., tadpole shrimp remains) macrofossils for this record at ~ CE 700 also suggests a less dynamic environment than P1 and P2 and low primary production in the aquatic network and terrestrial catchment, or transport of materials through regular

runoff (Gayo et al., 2012). Our multi-proxy record shows that these conditions persisted at the site until at least CE 1600 (Fig. 3).

3.2.1.4. Period 4 (P4)—CE <100–700: megadrought. The heavily compacted, homogeneous and dry silts of the sediment profile were underlain by a hard layer in the earliest section (48–61 cm), suggesting very low but steady accumulation rates that are consistent with prolonged droughts, in the order of decades to centuries (Fig. 3). Sediment total N and C contents were near or below detection limits (0.01 and 0.4%, respectively) during this period. Very low OM (<0.4% C) during this period indicates limited production, transport and/or preservation of materials in the pool and catchment. This low OM and N content also suggests the highest level of sub-aerial oxidation for the record, which we interpret as indicative of regular and prolonged drying (Fig. 3). 14 Mile Pool at this time would thus have been an episodic, clay pan-like system with a low-energy inundation regime. The absence of suitable macrofossils for dating precluded estimation of the onset of the core; tentative dating of bulk sediment samples also yielded incoherent age estimates. We thus conservatively estimate the arid conditions inferred in the Upper Fortescue River catchment to have spanned between CE < 100 and 700 in the record by extrapolating the age-depth models from P3. However, the age estimate extrapolated from Model 2 (Fig. 3) goes back as far as BCE 500, and together with the very dry, fine and compact lithology suggests that this record could be significantly older than estimated here. In addition, this period is likely to have been the most strongly affected by deflation creating hiatuses in the sequence due to the extremely dry conditions (Verschuren, 1999; Bristow et al., 2009), which could push back the onset even further towards the mid Holocene.

4. Discussion

4.1. Climate and environmental changes over the last ~2000 years

4.1.1. Period 1 (P1)—CE 1990 to present

The perennial aquatic depositional environment that we have reconstructed from the sediment indicators in P1 (post-1990) is consistent with regional instrumental rainfall data (Shi et al., 2008; Taschetto and England, 2009; Gallant and Karoly, 2010) and paleoclimatic reconstructions of increased rainfall (Cullen and Grierson, 2007; O'Donnell et al., 2015). Increased hydrological persistence of 14 Mile Pool over the last 20 years could be explained by a wetter and more reliable (less variable) rainfall regime resulting in limited supraseasonal droughts. In particular, this pattern of wetter conditions is consistent with the significant increase in annual hot and wet extremes and decrease in cold and dry extremes over the last century in northwest Australia (Gallant and Karoly, 2010).

At the larger scale, current moisture delivery in the Australian tropics and subtropics is influenced by several different interacting modes of interannual climate variability (Risbey et al., 2009; Fierro and Leslie, 2013; Frederiksen et al., 2014; Frederiksen and Grainger, 2015). Increased rainfall in northwest Australia in the late 1900s and early 2000s compared to the last 100–200 years has been attributed to shifts in cyclonic activity and tropical lows (Hassim and Walsh, 2008; Goebbert and Leslie, 2010; Lavender and Abbs, 2013; Kossin et al., 2014), and more broadly to an anomalously positive Southern Annular Mode (SAM) (Fierro and Leslie, 2013; Hendon et al., 2014; O'Donnell et al., 2015), enhanced La Niña conditions (Fierro and Leslie, 2013) and also to the warming of the Tropical Western Pacific Warm Pool (Lin and Li, 2012).

The southern annular mode (SAM), also referred to as the Antarctic Oscillation, has been anomalously positive over the last 60 years (Villalba et al., 2012; Abram et al., 2014). A positive phase of the SAM usually results in drier conditions in southwest and southeast Australia (Risbey et al., 2009); however, a positive phase of the SAM in summer and autumn can also drive wetter conditions in the subtropics, particularly northwest Australia. For example, Hendon et al. (2014) recently described the role of positive phases of the SAM during summer and autumn in driving 'eddy-induced divergent meridional circulation in the subtropics' and a poleward shift of the subtropical dry zone, resulting in higher precipitation in the subtropics. The significant link between the positive phase of the SAM and increased TC activity in the northwest of Australia was attributed to enhanced humidity and ascending motions (Mao et al., 2013). Interestingly, a recent tree-ring reconstruction from the Pilbara has also revealed strong correlations between the SAM and tree growth as well as with regional precipitation in summer and autumn (O'Donnell et al., 2015; Fig. 2b). Thus, a possible mechanism for the shift from P2 and P1 identified in the sediment record is a more positive SAM in this period; we would also infer that this influence of SAM was not as dominant in the previous 2000 years at least in the subtropical northwest.

4.1.2. Period 2 (P2)—CE 1600–1990

Collectively, the sedimentary evidence from the 14 Mile Pool suggests the P2 period was punctuated with one or multiple extreme flood(s) that would have been of much higher energy than any other period in the last ~2000 years. However, an overall increased rainfall for this period when compared to the most recent record (P1) is unlikely. Most of the events with sufficient intensity to cause the extreme floods are likely to originate from summer cyclonic rainfall (Rouillard et al., 2015). Hence conditions/drivers that would increase the genesis of TCs making land fall in the Pilbara likely peaked during at least one or more years. The onset of this period (P2) coincides with the onset of the LIA chronozone, where colder temperatures were recorded by high-resolution proxies between CE 1580 and 1880 in Australasia (PAGES 2k Consortium, 2013). Because the NH was colder still during the LIA, this period has been associated with a southward shift in the summer position of the ITCZ between CE 1400 and 1850 (Yancheva et al., 2007; Sachs et al., 2009; Tierney et al., 2010; Bird et al., 2011).

Under such a scenario, the rain belt of the ITCZ was likely pushed south of its modern position and many northern equatorial sites record extensive drought at that time (e.g., Sachs et al., 2009). The Pacific ITCZ is suggested to have been southward by as much as 5° during the LIA (Sachs et al., 2009). In the subtropical Pilbara, southward shifts or incursions might have been a primary force in bringing more intense TC rains in the summer (i.e., more southern location of TC genesis) that could have resulted in the extreme floods recorded here. During the peak LIA, southward shift in the ITCZ was inferred from 'wet' conditions observed south of contemporary summer latitudinal position in Africa (e.g., Verschuren, 2004), South America (Haug et al., 2001; Bird et al., 2011), the Pacific islands (Sachs et al., 2009) and (Indo-Pacific) eastern Australia/Australasia (Tierney et al., 2010; Burrows et al., 2014) while becoming drier northward. Though the influence of the ITCZ on rainfall has also been suggested for other cool periods of the late Quaternary for these regions, spatial inconsistencies in the African records have been identified from meta-analyses, highlighting the complexity of climatic systems and non-linearity in the environmental responses to hydroclimatic change and likely non-

stationarity on millennial timescales (Stager et al., 2011; Burrough and Thomas, 2013; Singarayer and Burrough, 2015).

Most TCs that landfall in the Pilbara are formed off the coast within the ITCZ thanks to favourable conditions brought together in the summer (Ramsay et al., 2012). Extreme floods during the LIA might have also been caused by the interaction of a more southern ITCZ (monsoonal trough) and strong La Niña events (Yan et al., 2011), also associated with tropical cyclogenesis and particularly wet summers in the northwest and northeast regions (Risbey et al., 2009; Goebbert and Leslie, 2010; Ramsay et al., 2012; Chand et al., 2013). However, recent evidence suggested that the MJO may have a more important role in TC genesis for this region compared to the ENSO than previously recognised (Hall et al., 2001; Leroy and Wheeler, 2008; Ramsay et al., 2012; Klotzbach, 2014; Klotzbach and Oliver, 2015). In particular, the positive phase of the MJO has been associated with increased TC activity in the southern Indian Ocean basin and along the northwest coast (Klotzbach and Oliver, 2015). In other basins, including the southwest Pacific, the MJO effects are typically overcome by the ENSO, but no strong relationship has been established of the combined effects of the MJO and ENSO on TCs for southern Indian Ocean basin (Klotzbach and Oliver, 2015). This evidence suggests that while particularly intense TCs in eastern Pilbara forming within a more southern ITCZ over the northwest coast may have caused the extreme floods of P2, the role of interannual large scale drivers of regional moisture delivery like the MJO may be underestimated.

Potentially contrasting evidence for our interpretation of P2 comes from the overall drier conditions during the LIA chronozone compared to the last ~1000 years inferred for a limited number of terrestrial records from the Australian tropics during the LIA chronozone, which have recently been attributed to shifts in the ENSO rather than migration of the ITCZ (Denniston et al., 2015; Yan et al., 2015). Assuming peat humification records indeed respond linearly to regional hydrological change (Yan et al., 2015) rather than local conditions (Burrows et al., 2014; Fig. 2), mean climatic state in the northeast tropics of Australia may have been drier during the LIA chronozone (Yan et al., 2015). Nevertheless, Burrows et al.'s study (2014) identified at least one regionally coherent wet shift during this period that could have been registered in the Fortescue Marsh record as extreme floods. Very few paleoecological records in northwest Australia have detailed information for the last 1000 years to enable further comparison (Yan et al., 2015; Fig. 2). Major peaks in fluvial activity on the millennial scale have also been recorded for the last 300 years in the Black Spring sediment core, collected inland in the Kimberley region (McGowan et al., 2012). The δ^{18}O-based speleothem record from the Kimberley coast suggests that during the Holocene, the Indonesian Australian summer monsoon (IASM) was at its lowest intensity (less monsoonal rain) between 2000 and 1000 years ago, and has been strengthening in intensity since (Denniston et al., 2013). In parallel, the 'mud layers' from the same speleothem sequence have been associated with extreme rainfall events brought by TCs suggesting reduced activity during CE 1450–1650 (Denniston et al., 2015). A significant hiatus in these two speleothem records during the LIA chronozone captured by the 14 Mile Pool core makes it difficult to assess further if reconstructed hydroclimate variables reflected a mean climatic state for this period or the occurrence of extremes such as the extreme floods. Our inferred extreme floods for the CE 1600–1990 period (P2) would be, however, consistent with a period of relatively high TC activity—with strong multi-decadal variability—reconstructed between CE 1600–1800 from a speleothem δ^{18}O record at Cape Range (northwest Australia) and Chillagoe (northeast Australia) (Haig et al., 2014). The speleothem-based index for TC activity developed at these locations was however, not correlated to rainfall and showed the lowest values for the respective records post-1960 (~P1).

High spatial variability in hydroclimatic conditions both at present and in the past across the vast tropical and sub-tropical region of Australia could also explain the differences in interpretation among records (Risbey et al., 2009; Singarayer and Burrough, 2015). For example, O'Donnell and al. (2015) showed that annual rainfall patterns in the last century from the Upper Fortescue catchment were not strongly correlated to the coastal rainfall regime of the Pilbara (i.e., Cape Range), nor with the broader tropics (Fig. 2b). Similarly, the development of additional late Holocene records of hydroclimatic conditions in summer rainfall dominated Africa is suggesting a higher spatial heterogeneity than previously thought (e.g., Stager et al., 2013; Woodborne et al., 2015). This disparity between periods and records in the northwest could also be explained by summertime rainfall being influenced by spatial shifts (i.e., more inland) in the tracks of the landfalling TCs and of other synoptic weather patterns (Berry et al., 2011; Ramsay et al., 2012), and/or that regional moisture delivery and dominant sources are influenced by the interaction between multiple large-scale forcing mechanisms discussed previously (Frederiksen and Grainger, 2015).

4.1.3. Period 3 (P3)—CE 700–1600

The relatively less intense but less variable hydrology (although drier overall than P1 and P2) from circa CE 700 in P3 is consistent with records showing a shift to decreased aridity at the onset of this period from the mid-Holocene between CE 700–1100 in the tropical northwest of Australia (McGowan et al., 2012; Fig. 2). As previously discussed, the relatively 'wet' conditions in the tropical north of the region during this period have been attributed to a progressive strengthening of the IASM post ~CE 1050 enabled by a weakening of the ENSO (Denniston et al., 2013). The weakening of the ENSO was consistent with TCs increasing, which could explain higher rainfall in the system (Nicholls, 1992). However, the monsoonal system acting as a primary mechanism for the delivery of moisture over the Pilbara at that time—as opposed to TCs—is consistent with the more northern position of the ITCZ (Yancheva et al., 2007; Sachs et al., 2009; PAGES 2k Consortium, 2013).

Our results show that CE 700–1600 (P3) was a prolonged period characterised by less vigorous but regular flows, episodically inundating a more ephemeral aquatic environment. Sediment at a site ~1000 km to the northeast of the Fortescue Marsh in the eastern Kimberley region (#5, Fig. 2a), also revealed a rapid increase in fluvial sedimentation around CE 650–850 concurrent with a more progressive increase in woody vegetation characteristic of the modern composition (McGowan et al., 2012). Recent analysis of speleothems from the Kimberley region and from Indonesia also shows that relatively wet conditions during the late Holocene were established following a relatively sharp transition between CE 750–1050 (Denniston et al., 2013). Consequently, the onset of relatively wetter conditions in the late Holocene from P3 at the 14 Mile Pool may have been linked to a change in hydroclimatic regime affecting the tropics and subtropics similarly.

This shift in regional climate of the northwest from ~CE 700 further appears to have been quite widespread in the Australian arid zone. For example, in central Australia (Northern Territory), extreme floods at the Ross River were recorded to have been more frequent during the late Holocene (i.e., CE 450–1250; Patton et al., 1993). Lower dust emissions (i.e., less dry) from the Lake Eyre Basin at CE 1100 were also attributed to a decrease in climate variability (decrease in ENSO activity), though concurrent change in aridity

was not clear (Marx et al., 2009). Climatic amelioration and enhanced growth of vegetation in the arid zone are also reflected by a wealth of evidence from the archaeological literature supporting models of increased regional occupation between ~CE 500–1000 (Smith and Ross, 2008; Smith et al., 2008; McDonald and Veth, 2013; Williams, 2013; Williams et al., 2015).

4.1.4. Period 4 (P4)—CE <100–700

The hyperarid conditions inferred in P4 appear quite coherent throughout the Australian arid zones from ~5000 calibrated years before present (cal yrs BP) (Hesse et al., 2004; Marx et al., 2009; Denniston et al., 2013; Reeves et al., 2013a, b). The analysis of a 6500-year long record of combined pollen and aeolian dust from the Kimberley region revealed a 'megadrought' (~1500 years long) had been ongoing in the Australian northwest since 2400 cal yrs BP/CE −450 (McGowan et al., 2012; Fig. 2). Less frequent and shorter-lived wet shifts were identified in the northeast tropics from peat humification records prior to ~ CE 500 (Burrows et al., 2014). These studies support conclusions from early work on the formation of cheniers and sand dunes from northern Australian tropical rivers, which also identified a particularly dry period during the 2800–1600 cal yrs BP/CE −850 to 350, with suggestions that this could be as early as 3800 cal yrs BP/CE −1850 (Lees, 1992; Shulmeister and Lees, 1995). The evidence included wide-ranging declines in effective precipitation, lake levels (Shulmeister and Lees, 1995) and fluvial discharge (Lees, 1992). Increasingly arid conditions from the mid-Holocene to ~1500 years ago in the northwest were also recently corroborated from a multi-proxy investigation of deep-sea sediment off the Pilbara coast (De Deckker et al., 2014), coastal Kimberley sediment (Proske et al., 2014), and from multiple Australasian speleothem records (Denniston et al., 2013), confirming that drought was widespread across the region. This aridification across northern Australia has been linked to particularly strong ENSO cycles and related failure of the monsoonal system, resulting in enhanced climatic variability (Denniston et al., 2013; De Deckker et al., 2014).

5. Conclusions

This study provides the first sedimentological evidence from the Pilbara revealing major hydrological changes have taken place in the arid subtropics of northwest Australia over the last 2000 years, including phases of extremely wet conditions (resulting from extreme floods) as well as an extended drought more than 1000 years ago. The paleolimnological reconstruction for the most recent ~20 years is consistent with the instrumental record, with 14 Mile Pool—the most regularly inundated pool of the Fortescue Marsh today—becoming near perennial for what appears the first time in the record. Importantly, the sediment stratigraphy reveals that extreme floods occurred in the period CE 1600–1990, which is broadly synchronous with the LIA chronozone. The results from our reconstruction are consistent with other records of wetter climes or at least of high intensity wet peaks for the SH that have been linked to a southward shift in the ITCZ and/or more pervasive La Niña-like conditions, but may also be more specifically due to the influence of other regional hydroclimatic drivers on tropical cyclogenesis such as the MJO. For the earlier sections of the sedimentary sequence, we show that the eastern Pilbara responded until circa CE 700 to a megadrought pervasive in most of the Australian arid zone and originating in the mid Holocene, which was followed by climatic amelioration likely related to weakening of the ENSO and strengthening of monsoonal patterns. The results suggest that the dominant forcing mechanisms of moisture delivery on the arid northwest Australian landscape have not been stationary over the last 2000 years.

Overall, we show that the increased seasonality of rainfall over the last 2000 years was experienced in the Marsh with the catchment becoming 'wetter' (increasing the recharge), demonstrating the importance of establishing the variability of a system and not just its long-term average climatic conditions. We suggest that the increased difference among paleohydrological records from the northwest, northern tropics and northeast tropical and sub-tropical Australian regions during the late Holocene may have been due to non-stationarity in the strength of large-scale forcing mechanisms on TC genesis location, direction of tracks, frequency and intensity (through ITCZ, ENSO, MJO and/or SAM). Further work developing paleohydrological records from the Australian tropics and subtropics is crucial for refining our understanding of these competing modes of variability and their likely behaviour under future scenarios. By providing a baseline of hydrological change, the findings from our study have implications for exploring past and potential future changes in the drivers of moisture in subtropical drylands. These results also provide a window for appraising how water-limited ecosystems that have proved resilient through significant shifts in hydrology over the recent past might cope with increasing land-use pressures and/or altered hydrological variability in the future.

Acknowledgements

We thank David Thomas (Oxford University), Dirk Verschuren (Ghent University) and John Tibby (University of Adelaide) for their thorough and constructive comments on an early draft as well as our two anonymous reviewers, which have helped focus and improve the quality of the paper. This research was supported by the Australian Research Council in partnership with Rio Tinto (LP120100310) and by Australian Institute of Nuclear Science and Engineering (AINSE) (ALNGRA13043). A. Rouillard was supported by an International Postgraduate Research Scholarship (IPRS), an Australian Postgraduate Award (APA), and Natural Sciences and Engineering Research Council (NSERC) and Fonds Québécois de la Recherche sur la Nature et les Technologies (FQRNT) graduate scholarships. G. Skrzypek was supported by an ARC Future Fellowship (FT110100352) and C. Turney by a Laureate Fellowship (FL100100195). We thank Glenn Kirkpatrick, Douglas Ford, Ray Scott and Bill Wilson for field and technical support. We are grateful to Fortescue Metals Group Ltd for providing access to orthoimagery, digital elevation model (DEM) and field sites. The high-resolution dry image of the core was provided by the Geological Survey of Western Australia. We also acknowledge the kind field support of Murray and Ray Kennedy (Roy Hill Station), Sue and Lee Bickell (Marillana Station), Barry and Bella Grett (Ethel Creek Station) and Victor and Larissa Gleeson (Mulga Downs Station). We thank Charlotte Cook (UNSW) and John Tibby (Uni. Adelaide) for preliminary assessment of pollen and diatom samples. Screening for chironomids and identification was kindly conducted by Wetland Resources Management (Perth, Australia). Patrick De Deckker (ANU) and Stuart Halse (Bennelongia Pty Ltd) helped with early ostracod identification and Todd Erickson (UWA) provided seed identification. We also thank Gavan McGrath, Nik Callow (UWA), Caroline Bird (Archae-Aus), Simon Haberle (ANU), Jonathan Palmer (UNSW), Adrienne Marquis (DPaW) for their useful and generous advice.

Appendix

Table A.1
Results of AMS ^{14}C analyses used to derive the two age models. The unmodelled ages (*OxCal* v. 4.2; Bronk Ramsey, 2009) are provided in calibrated Common Era years (cal CE yrs); the two sigma (2σ) age range of the distributions with the highest probability density is provided. Results from bulk sediment were excluded from the age models due to the variable reservoir ages obtained. Sample depths of replicate core FOR106C2 were converted to FOR106C3 for calculations using visual layering of the sequences. Samples with the prefix 'OZ' and 'Wk-' were prepared and dated at ANSTO and the Waikato University, respectively.

Type	Core	Sample type	Lab ID	FOR106C3 depth (cm)	FOR106C2 depth (cm)	δ^{13}C (‰ VPDB)	pMC		^{14}C conv. age (BP)		Reservoir age (^{14}C yr)		Unmodelled age (cal CE yrs)	
							Mean	1σ	Mean	1σ	Mean	1σ	Median	2σ age range
Macrofossils	FOR106C2	Terrestrial plant material	OZR585	8–9[a]	8–9	−24.7	105.78	0.29	Modern				1957	1957–1958
													2009	2007–2011
	FOR106C2	Terrestrial plant material	OZQ883	19–20[a]	18–19	−26.4	108.57	0.41	Modern				1958	1957–1959
													2002	2000–2004
	FOR106C3	Terrestrial plant material	OZQ887	23–24		−25.6	126.29	0.34	Modern				1962	1962–1963
													1981	1980–1982
	FOR106C3	Charred wood	OZQ888	31–32		−26.1	97.18	0.29	230	24			1757	1650–1954
	FOR106C3	Terrestrial plant seed	Wk–35517	35–36		−23.7	97.63	0.32	193	26			1768	1665–1955
	FOR106C3	Charred wood	OZQ891	39–40		−25.4	98.42	0.43	128	35			1855	1683–1955
	FOR106C2	Charred wood	OZR586	44–45[a]	49–50	−25.0[b]	84.64	0.79	1340	75			744	603–951
	FOR106C2	Charred wood	OZQ884	47–48[a]	53–54	−25.0[b]	85.36	0.86	1272	81			809	660–976
Bulk sediment	FOR106C3	Bulk sediment	OZQ886	23–24		−22.0	122.58	0.47	Modern		240	38		
	FOR106C3	Bulk sediment	OZQ889	35–36		−19.9	88.54	0.34	978	31	785	40		
	FOR106C3	Bulk sediment	OZQ890	39–40		−19.8	72.25	0.31	2611	34	2483	49		
	FOR106C3	Bulk sediment	OZQ892	53–54		−25.0[b]	23.60	0.39	11,600	140				
	FOR106C3	Bulk sediment	OZQ893	59–60		−25.0[b]	23.63	0.32	11,590	110				
	FOR106C2	Bulk sediment	OZQ885	60–61[a]	64–65	−24.6	17.07	0.21	14,200	100				

Note:
[a] Equivalent FOR106C3.
[b] Assumed δ^{13}C value as no measured δ^{13}C was available due to low carbon mass.

Table A.2
Modelled ages provided in calibrated Common Era years (cal CE yrs) corresponding to AMS ^{14}C dated samples using Bayesian P_Sequence Model 1 (*OxCal* v. 4.2; Bronk Ramsey, 2009) and Smooth Spline Fitting Model 2 (*CLAM*; Blaauw, 2010), with respective 95% confidence intervals.

Depth (cm)	Modelled Age (cal CE yrs) – Model 1 *OxCal*			Modelled Age (cal CE yrs) – Model 2 *Clam*		
	Median	max95%	min95%	Best	max95%	min95%
8–9	2008	2007	2010	2005	1999	2009
18–19	1999	1987	2004	1986	1981	1992
23–24	1981	1962	1982	1980	1974	1987
31–32	1786	1742	1806	1908	1886	1922
35–36	1739	1694	1782	1778	1729	1821
39–40	1696	1672	1725	1548	1453	1645
49–50[a]	772	633	911	691	520	971
53–54[a]	672	533	839	335	120	683

Note: Depths corresponding to ages obtained from FOR106C2 have been provided as FOR106C3 equivalents.
[a] Linearly extrapolated.

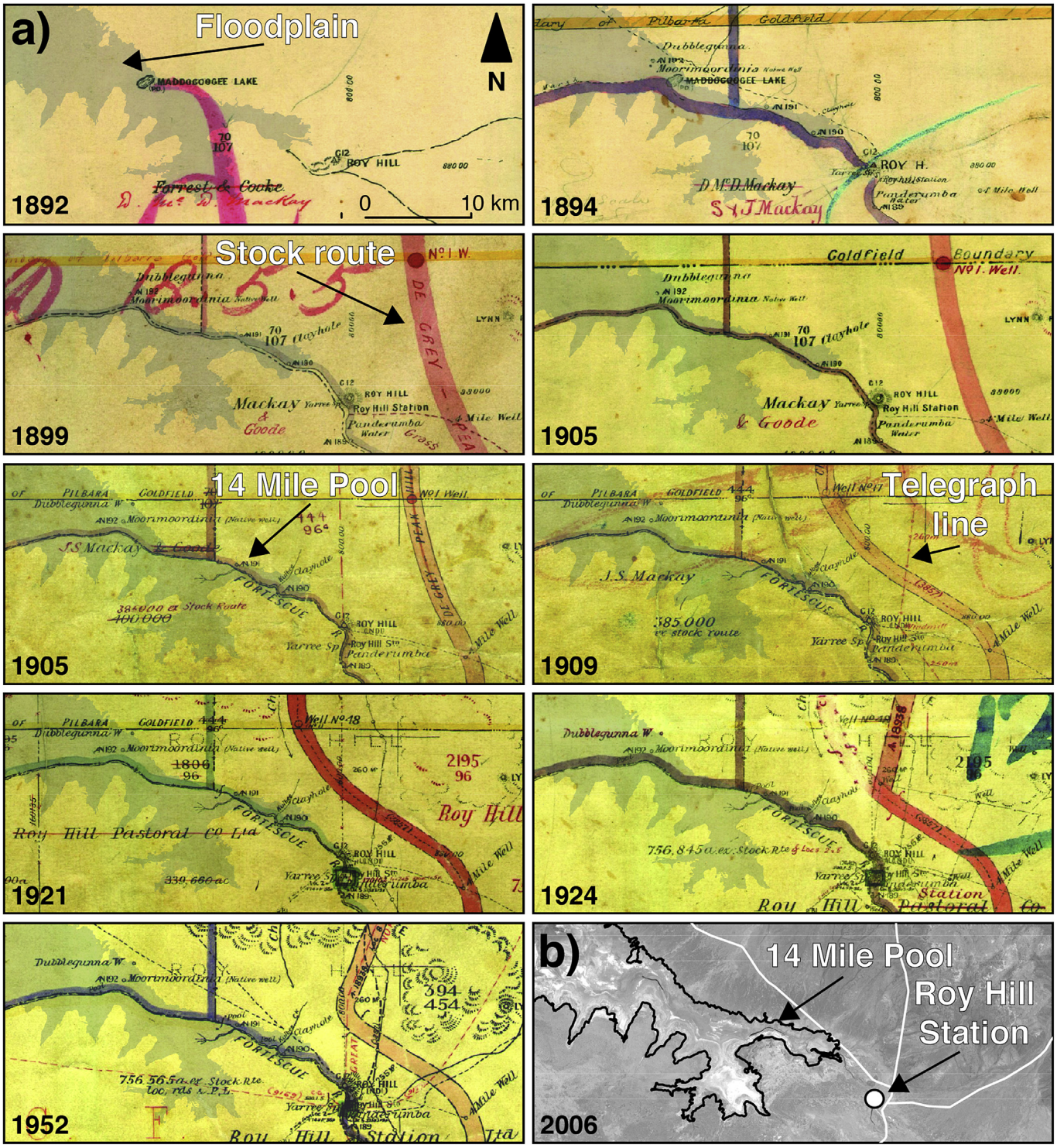

Fig. A.1. Historical land use surrounding 14 Mile Pool (1892–2010) from **a)** a public plans series ortho-rectified for the purpose of this study using landmarks (Dept Land and Surveys, 1892, 1894, 1899, 1905a,b, 1909, 1919, 1921, 1924, 1952) overlaid with the Fortescue Marsh floodplain (shaded blue area; modified from Rouillard et al., 2015; USGS) and **b)** recent satellite image (Dec 2006; SPOT–5) showing the 14 Pool bed (darker linear shape), with the Fortescue Marsh floodplain (solid black line) and roads (solid white line).

References

Abram, N.J., Mulvaney, R., Vimeux, F., Phipps, S.J., Turner, J., England, M.H., 2014. Evolution of the Southern Annular Mode during the past millennium. Nat. Clim. Change 4, 564–569.

Adair, E.C., Burke, I.C., 2010. Plant phenology and life span influence soil pool dynamics: *Bromus tectorum* invasion of perennial C_3-C_4 grass communities. Plant Soil 335, 255–269.

Appleby, P.G., 2001. Chronostratigraphic techniques in recent sediments. In: Last, W.M., Smol, J.P. (Eds.), Basin Analysis, Coring, and Chronological Techniques, vol. 1. Springer, Dordrecht, pp. 171–203.

Baird, W., 1843. Notes on the British Entomostraca. Zoologist 1, 193–197.

Battin, T.J., Kaplan, L.A., Findlay, S., Hopkinson, C.S., Marti, E., Packman, A.I., Newbold, J.D., Sabater, F., 2008. Biophysical controls on organic carbon fluxes in fluvial networks. Nat. Geosci. 1, 95–100.

Beard, J.S., 1975. The Vegetation of the Pilbara Area. Vegetation Survey of Western Australia, 1: 1000000 Vegetation Series, Map and Explanatory Notes. The University of Western Australia Press, Nedlands.

Berry, G., Reeder, M.J., Jakob, C., 2011. Physical mechanisms regulating summertime rainfall over northwestern Australia. J. Clim. 24, 3705–3717.

Bessems, I., Verschuren, D., Russell, J.M., Hus, J., Mees, F., Cumming, B.F., 2008. Palaeolimnological evidence for widespread late 18th century drought across equatorial East Africa. Palaeogeogr. Palaeoclimatol. Palaeoecol. 259, 107–120.

Bird, B.W., Abbott, M.B., Vuille, M., Rodbell, D.T., Stansell, N.D., Rosenmeier, M.F., 2011. A 2,300-year-long annually resolved record of the South American summer monsoon from the Peruvian Andes. Proc. Natl. Acad. Sci. 108, 8583–8588.

Björck, S., Wohlfarth, B., 2001. ^{14}C chronostratigraphic techniques in paleolimnology. In: Last, W.M., Smol, J.P. (Eds.), Basin Analysis, Coring, and Chronological Techniques, vol. 1. Springer, Dordrecht, pp. 205–245.

Blaauw, M., 2010. Methods and code for 'classical' age-modelling of radiocarbon sequences. Quat. Geochronol. 5, 512–518.

Blott, S.J., Pye, K., 2001. GRADISTAT: a grain size distribution and statistics package for the analysis of unconsolidated sediments. Earth Surf. Process. Landf. 26, 1237–1248.

Brahney, J., Ballantyne, A.P., Turner, B.L., Spaulding, S.A., Otu, M., Neff, J.C., 2014. Separating the influences of diagenesis, productivity and anthropogenic nitrogen deposition on sedimentary δ^{15}N variations. Org. Geochem. 75, 140–150.

Brenner, M., Whitmore, T.J., Curtis, J.H., Hodell, D.A., Schelske, C.L., 1999. Stable isotope (δ^{13}C and δ^{15}N) signatures of sedimented organic matter as indicators of historic lake trophic state. J. Paleolimnol. 22, 205–221.

Bristow, C.S., Drake, N., Armitage, S., 2009. Deflation in the dustiest place on Earth: the Bodélé Depression, Chad. Geomorphology 105, 50–58.

Broccoli, A.J., Dahl, K.A., Stouffer, R.J., 2006. Response of the ITCZ to Northern Hemisphere cooling. Geophys. Res. Lett. 33.

Brodie, C.R., Casford, J.S.L., Lloyd, J.M., Leng, M.J., Heaton, T.H.E., Kendrick, C.P., Yongqiang, Z., 2011. Evidence for bias in C/N, δ^{13}C and δ^{15}N values of bulk organic matter, and on environmental interpretation, from a lake sedimentary sequence by pre-analysis acid treatment methods. Quat. Sci. Rev. 30, 3076–3087.

Bronk Ramsey, C., 2008. Deposition models for chronological records. Quat. Sci. Rev. 27, 42–60.

Bronk Ramsey, C., 2009. Bayesian analysis of radiocarbon dates. Radiocarbon 51, 337–360.

Burrough, S.L., Thomas, D.S.G., 2013. Central southern Africa at the time of the African Humid Period: a new analysis of Holocene palaeoenvironmental and palaeoclimate data. Quat. Sci. Rev. 80, 29–46.

Burrows, M.A., Fenner, J., Haberle, S.G., 2014. Humification in northeast Australia: dating millennial and centennial scale climate variability in the late Holocene. The Holocene 1–12.

Chand, S.S., Tory, K.J., McBride, J.L., Wheeler, M.C., Dare, R.A., Walsh, K.J.E., 2013. The different impact of positive-neutral and negative-neutral ENSO regimes on Australian tropical cyclones. J. Clim. 26, 8008–8016.

Coianiz, L., Ariztegui, D., Piovano, E.L., Lami, A., Guilizzoni, P., Gerli, S., Waldmann, N., 2015. Environmental change in subtropical South America for the last two millennia as shown by lacustrine pigments. J. Paleolimnol. 53, 233–250.

Cullen, L.E., Grierson, P.F., 2007. A stable oxygen, but not carbon, isotope chronology of *Callitris columellaris* reflects recent climate change in north-western Australia. Clim. Change 85, 213–229.

Cuna, E., Zawisza, E., Caballero, M., Ruiz-Fernández, A.C., Lozano-García, S., Alcocer, J., 2014. Environmental impacts of Little Ice Age cooling in central Mexico recorded in the sediments of a tropical alpine lake. J. Paleolimnol. 51, 1–14.

Cushing, E.J., 1967. Evidence for differential pollen preservation in late Quaternary sediments in Minnesota. Rev. Palaeobot. Palynol. 4, 87–101.

Dare, R.A., Davidson, N.E., McBride, J.L., 2012. Tropical cyclone contribution to rainfall over Australia. Mon. Weather Rev. 140, 3606–3619.

De Deckker, P., Barrows, T.T., Rogers, J., 2014. Land-sea correlations in the Australian region: post-glacial onset of the monsoon in northwestern Western Australia. Quat. Sci. Rev. 105, 181–194.

Denniston, R.F., Villarini, G., Gonzales, A.N., Wyrwoll, K.-H., Polyak, V.J., Ummenhofer, C.C., Lachniet, M.S., Wanamaker, A.D., Humphreys, W.F., Woods, D., others, 2015. Extreme rainfall activity in the Australian tropics reflects changes in the El Niño/Southern Oscillation over the last two millennia. Proc. Natl. Acad. Sci. 112, 4576–4581.

Denniston, R.F., Wyrwoll, K.-H., Polyak, V.J., Brown, J.R., Asmerom, Y., Wanamaker, J., Alan, D., LaPointe, Z., Ellerbroek, R., Barthelmes, M., Cleary, D., others, 2013. A Stalagmite record of Holocene Indonesian-Australian summer monsoon variability from the Australian tropics. Quat. Sci. Rev. 78, 155–168.

Department of Lands and Surveys, 1892. 1892–94 North West [Tally No. 505580]. Cancelled Public Plans 1878–1907 (Standard Series), State Records Office of Western Australia (SROWA) Acc 541. Available from: http://aeon.sro.wa.gov.au (8 April 2015).

Department of Lands and Surveys, 1894. 1894 North West [Tally No. 505581]. Cancelled Public Plans 1878–1907 (Standard Series), State Records Office of Western Australia (SROWA) Acc 541. Available from: http://aeon.sro.wa.gov.au (8 April 2015).

Department of Lands and Surveys, 1899. 1899–1905 North West [Tally No. 505582]. Cancelled Public Plans 1878–1907 (Standard Series), State Records Office of Western Australia (SROWA) Acc 541. Available from: http://aeon.sro.wa.gov.au (8 April 2015).

Department of Lands and Surveys, 1905a. 1905–05 300 Chain Plan [Tally No. 503157]. Cancelled Public Pans 1903–1965 (Original State Series; 300 Chain Plans), State Records Office of Western Australia (SROWA) Acc 541. Available from: http://aeon.sro.wa.gov.au (8 April 2015).

Department of Lands and Surveys, 1905b. 1905–09 300 Chain Plan [Tally No. 503158]. Cancelled Public Pans 1903–1965 (Original State Series; 300 Chain Plans), State Records Office of Western Australia (SROWA) Acc 541. Available from: http://aeon.sro.wa.gov.au (8 April 2015).

Department of Lands and Surveys, 1909. 1909–16 300 Chain Plan [Tally No. 503159]. Cancelled Public Pans 1903–1965 (Original State Series; 300 Chain Plans), State Records Office of Western Australia (SROWA) Acc 541. Available from: http://aeon.sro.wa.gov.au (8 April 2015).

Department of Lands and Surveys (1919) File 1919/05125: Letter Athol J. Bennett to Surveyor General, 05/09/1919. Surveys by Roy Hill Pastoral Co in Victoria district of Roy Hill Station, Folio 13, State Records Office of Western Australia (SROWA) Acc 541.

Department of Lands and Surveys, 1921. 1921–24 300 Chain Plan [Tally No. 503161]. Cancelled Public Pans 1903–1965 (Original State Series; 300 Chain Plans), State Records Office of Western Australia (SROWA) Acc 541. Available from: http://aeon.sro.wa.gov.au (8 April 2015).

Department of Lands and Surveys, 1924. 1924–29 300 Chain Plan [Tally No. 503162]. Cancelled Public Pans 1903–1965 (Original State Series; 300 Chain Plans), State Records Office of Western Australia (SROWA) Acc 541. Available from: http://aeon.sro.wa.gov.au (8 April 2015).

Department of Lands and Surveys, 1952. 1952–61 300 Chain Plan [Tally No. 503164]. Cancelled Public Pans 1903–1965 (Original State Series; 300 Chain Plans), State Records Office of Western Australia (SROWA) Acc 541. Available from: http://aeon.sro.wa.gov.au (8 April 2015).

Donselaar, M.E., Gozalo, C., Moyano, S., 2013. Avulsion processes at the terminus of low-gradient semi-arid fluvial systems: lessons from the Río Colorado, Altiplano endorheic basin, Bolivia. Sediment. Geol. 283, 1–14.

Dunne, T., Western, D., Dietrich, W.E., 2011. Effects of cattle trampling on vegetation, infiltration, and erosion in a tropical rangeland. J. Arid Environ. 75, 58–69.

Eldridge, D.J., Koen, T.B., Killgore, A., Huang, N., Whitford, W.G., 2012. Animal foraging as a mechanism for sediment movement and soil nutrient development: evidence from the semi-arid Australian woodlands and the Chihuahuan Desert. Geomorphology 157, 131–141.

Fierro, A.O., Leslie, L.M., 2013. Links between Central West Western Australian rainfall variability and large-scale climate drivers. J. Clim. 26, 2222–2245.

Fink, D., Hotchkis, M., Hua, Q., Jacobsen, G., Smith, A.M., Zoppi, U., Child, D., Mifsud, C., van der Gaast, H., Williams, A., et al., 2004. The ANTARES AMS facility at ANSTO. Nucl. Instrum. Methods Phys. Res. Sect. B Beam Interact. Mater. Atoms 223, 109–115.

Finlay, J.C., Kendall, C., 2008. Stable isotope tracing of temporal and spatial variability in organic matter sources to freshwater ecosystems. In: Michener, R., Lajtha, K. (Eds.), Stable Isotopes in Ecology and Environmental Science. Wiley-Blackwell, Oxford, UK, pp. 283–333. Hoboken.

Fitzsimmons, K.E., Cohen, T.J., Hesse, P.P., Jansen, J., Nanson, G.C., May, J.-H., Barrows, T.T., Haberlah, D., Hilgers, A., Kelly, T., others, 2013. Late Quaternary palaeoenvironmental change in the Australian drylands. Quat. Sci. Rev. 74, 78–96.

Frederiksen, C.S., Grainger, S., 2015. The role of external forcing in prolonged trends in Australian rainfall. Clim. Dyn. 45, 2455–2468.

Frederiksen, C.S., Zheng, X., Grainger, S., 2014. Teleconnections and predictive characteristics of Australian seasonal rainfall. Clim. Dyn. 43, 1381–1408.

Ford, D.J., Cookson, W.R., Adams, M.A., Grierson, P.F., 2007. Role of soil drying in nitrogen mineralization and microbial community function in semi-arid grasslands of north-west Australia. Soil Biol. Biochem. 39, 1557–1569.

Gallant, A.J.E., Karoly, D.J., 2010. A combined climate extremes index for the Australian region. Bull. Am. Meteorol. Society 23, 6153–6165.

Gälman, V., Rydberg, J., Bigler, C., 2009. Decadal diagenetic effects on δ^{13}C and δ^{15}N studied in varved lake sediment. Limnol. Oceanogr. 54, 917–924.

Gayo, E.M., Latorre, C., Santoro, C.M., Maldonado, A., De Pol-Holz, R., 2012. Hydroclimate variability in the low-elevation Atacama Desert over the last 2500 yr. Clim. Past 8, 287–306.

Gell, P.A., Bulpin, S., Wallbrink, P., Hancock, G., Bickford, S., 2005. Tareena Billabong - a palaeolimnological history of an ever-changing wetland, Chowilla Floodplain, lower Murray-Darling basin, Australia. Mar. Freshw. Res. 56, 441–456.

Goebbert, K.H., Leslie, L.M., 2010. Interannual variability of Northwest Australian

tropical cyclones. J. Clim. 23, 4538–4555.
Graham, N.E., Ammann, C.M., Fleitmann, D., Cobb, K.M., Luterbacher, J., 2011. Support for global climate reorganization during the "Medieval Climate Anomaly". Clim. Dyn. 37, 1217–1245.
Haig, J., Nott, J., Reichart, G.-J., 2014. Australian tropical cyclone activity lower than at any time over the past 550-1,500 years. Nature 505, 667–671.
Hall, J.D., Matthews, A.J., Karoly, D.J., 2001. The modulation of tropical cyclone activity in the Australian region by the Madden-Julian Oscillation. Mon. Weather Rev. 129, 2970–2982.
Hassim, M.E.E., Walsh, K.J.E., 2008. Tropical cyclone trends in the Australian region. Geochem. Geophys. Geosyst. 9.
Haug, G.H., Hughen, K.A., Sigman, D.M., Peterson, L.C., Röhl, U., 2001. Southward migration of the intertropical convergence zone through the Holocene. Science 293, 1304–1308.
Hendon, H.H., Lim, E.-P., Nguyen, H., 2014. Seasonal variations of subtropical precipitation associated with the southern annular mode. J. Clim. 27, 3446–3460.
Hesse, P.P., Magee, J.W., van der Kaars, S., 2004. Late Quaternary climates of the Australian arid zone: a review. Quat. Int. 118, 87–102.
Hodell, D.A., Brenner, M., Curtis, J.H., Medina-González, R., Can, E.I.-C., Albornaz-Pat, A., Guilderson, T.P., 2005. Climate change on the Yucatan Peninsula during the Little Ice Age. Quat. Res. 63, 109–121.
Hogg, A.G., Hua, Q., Blackwell, P.G., Niu, M., Buck, C.E., Guilderson, T.P., Heaton, T.J., Palmer, J.G., Reimer, P.J., Reimer, R.W., others, 2013. SHCal13 Southern Hemisphere calibration, 0-50,000 cal yr BP. Radiocarbon 55, 1889–1903.
Hua, Q., Jacobsen, G.E., Zoppi, U., Lawson, E.M., Williams, A.A., Smith, A.M., McGann, M.J., 2001. Progress in radiocarbon target preparation at the ANTARES AMS Centre. Radiocarbon 43, 275–282.
Hua, Q., Barbetti, M., Rakowski, A.Z., 2013. Atmospheric radiocarbon for the period 1950-2010. Radiocarbon 55, 2059–2072.
Jenkins, K.M., Boulton, A.J., 2003. Connectivity in a dryland river: short-term aquatic microinvertebrate recruitment following floodplain inundation. Ecology 84, 2708–2723.
Jones, L.S., Schumm, S.A., 2009. Causes of avulsion: an overview. Fluv. Sedimentol. VI, 171–178.
Karanovic, I., 2008. Three interesting Cyprididae (Ostracoda) from Western Australia. Rec. West. Aust. Mus. 24, 267–287.
Kennard, M.J., Pusey, B.J., Olden, J.D., Mackay, S.J., Stein, J.L., Marsh, N., 2010. Classification of natural flow regimes in Australia to support environmental flow management. Freshw. Biol. 55, 171–193.
Klotzbach, P.J., 2014. The Madden-Julian Oscillation's impacts on worldwide tropical cyclone activity. J. Clim. 27, 2317–2330.
Klotzbach, P.J., Oliver, E.C.J., 2015. Variations in global tropical cyclone activity and the Madden-Julian Oscillation since the Mid-20th century. Geophys. Res. Lett. 42, 4199–4207.
Kossin, J.P., Emanuel, K.A., Vecchi, G.A., 2014. The poleward migration of the location of tropical cyclone maximum intensity. Nature 509, 349–352.
Lavender, S.L., Abbs, D.J., 2013. Trends in Australian rainfall: contribution of tropical cyclones and closed lows. Clim. Dyn. 40, 317–326.
Lees, B.G., 1992. Geomorphological evidence for late Holocene climatic change in northern Australia. Aust. Geogr. 23, 1–10.
Leroy, A., Wheeler, M.C., 2008. Statistical prediction of weekly tropical cyclone activity in the Southern Hemisphere. Mon. Weather Rev. 136, 3637–3654.
Leslie, C., Hancock, G.J., 2008. Estimating the date corresponding to the horizon of the first detection of ^{137}Cs and $^{239+240}$Pu in sediment cores. J. Environ. Radioact. 99, 483–490.
Lin, Z., Li, Y., 2012. Remote influence of the tropical Atlantic on the variability and trend in North West Australia summer rainfall. J. Clim. 25, 2408–2420.
Lowe, J.J., 1982. Three flandrian pollen profiles from the Teith Valley, Perthshire, Scotland. II. Analysis of deteriorated pollen. New Phytol. 90, 371–385.
Mao, R., Gong, D.-Y., Yang, J., Zhang, Z.-Y., Kim, S.-J., He, H.-Z., 2013. Is there a linkage between the tropical cyclone activity in the southern Indian Ocean and the Antarctic Oscillation? J. Geophys. Res. Atmos. 118, 8519–8535.
Marx, S.K., McGowan, H.A., Kamber, B.S., 2009. Long-range dust transport from eastern Australia: a proxy for Holocene aridity and ENSO-type climate variability. Earth Planet. Sci. Lett. 282, 167–177.
Masson-Delmotte, V., Schulz, M., Abe-Ouchi, A., Beer, J., Ganopolski, A., González Rouco, J.F., Jansen, E., Lambeck, K., Luterbacher, J., Naish, T., Osborn, T., Otto-Bliesner, B., Quinn, T., Ramesh, R., Rojas, M., Shao, X., Timmermann, A., 2013. Information from Paleoclimate archives. In: Stocker, T., Qin, D., Plattner, G.-K., Tignor, M., Allen, S.K., Boschung, J., Nauels, A., Xia, Y., Bex, V., Midgley, P.M. (Eds.), Climate Change 2013: the Physical Science Basis. Contribution of Working Group I to the Fifth Assessment Report of the Intergovernmental Panel on Climate Change. Cambridge University Press, Cambridge, UK, and New York, pp. 383–464.
McBride, J.L., Keenan, T.D., 1982. Climatology of tropical cyclone genesis in the Australian region. J. Climatol. 2, 13–33.
McDonald, J., Veth, P., 2013. Rock art in arid landscapes: Pilbara and Western Desert petroglyphs. Aust. Archaeol. 66.
McGowan, H., Marx, S., Moss, P., Hammond, A., 2012. Evidence of ENSO mega-drought triggered collapse of prehistory Aboriginal society in northwest Australia. Geophys. Res. Lett. 39.
McIntyre, R.E.S., Adams, M.A., Ford, D.J., Grierson, P.F., 2009a. Rewetting and litter addition influence mineralisation and microbial communities in soils from a semi-arid intermittent stream. Soil Biol. Biochem. 41, 92–101.
McIntyre, R.E.S., Adams, M.A., Grierson, P.F., 2009b. Nitrogen mineralization potential in rewetted soils from a semi-arid stream landscape, north-west Australia. J. Arid Environ. 73, 48–54.
McKenzie, N.L., van Leeuwen, S., Pinder, A.M., 2009. Introduction to the Pilbara biodiversity survey, 2002-2007. Rec. West. Aust. Mus. (Suppl. 78), 3–89.
Mohtadi, M., Prange, M., Oppo, D.W., De, P.-H., Ricardo, Merkel U., Zhang, X., Steinke, S., Lückge, A., 2014. North Atlantic forcing of tropical Indian Ocean climate. Nature 509, 76–80.
Neukom, R., Gergis, J., 2012. Southern Hemisphere high-resolution palaeoclimate records of the last 2000 years. The Holocene 22, 501–524.
Ng, B., Walsh, K., Lavender, S., 2015. The contribution of tropical cyclones to rainfall in northwest Australia. Int. J. Climatol. 35, 2689–2697.
Nicholls, N., 1992. Recent performance of a method for forecasting Australian seasonal tropical cyclone activity. Aust. Meteorol. Mag. 40, 105–110.
O'Donnell, A.J., Cook, E.R., Palmer, J.G., Turney, C.S.M., Page, G.F.M., Grierson, P.F., 2015. Tree rings show recent high summer-autumn precipitation in northwest Australia is unprecedented within the last two centuries. PloS one 10, e0128533.
PAGES 2k Consortium, Ahmed, M., Anchukaitis, K.J., Asrat, A., Borgaonkar, H.P., Braida, M., Buckley, B.M., Büntgen, U., Chase, B.M., Christie, D.A., Cook, E.R., Curran, M.A.J., Diaz, H.F., Esper, J., Fan, Z.-X., Gaire, N.P., Ge, Q., Gergis, J., González-Rouco, J.F., Goosse, H., Grab, S.W., Graham, N., Graham, R., Grosjean, M., Hanhijärvi, S.T., Kaufman, D.S., Kiefer, T., Kimura, K., Korhola, A.A., Krusic, P.J., Lara, A., Lézine, A.-M., Ljungqvist, F.C., Lorrey, A.M., Luterbacher, J., Masson-Delmotte, V., McCarroll, D., McConnell, J.R., McKay, N.P., Morales, M.S., Moy, A.D., Mulvaney, R., Mundo, I.A., Nakatsuka, T., Nash, D.J., Neukom, R., Nicholson, S.E., Oerter, H., Palmer, J.G., Phipps, S.J., Prieto, M.R., Rivera, A., Sano, M., Severi, M., Shanahan, T.M., Shao, X., Shi, F., Sigl, M., Smerdon, J.E., Solomina, O.N., Steig, E.J., Stenni, B., Thamban, M., Trouet, V., Turney, C.S.M., Umer, M., van Ommen, T., Verschuren, D., Viau, A.E., Villalba, R., Vinther BM, von Gunten, L., Wagner, S., Wahl, E.R., Wanner, H., Werner, J.P., White, J.W.C., Yasue, K., Zorita, E., 2013. Continental-scale temperature variability during the past two millennia. Nat. Geosci. 6, 339–346.
Palmer, J.G., Cook, E.R., Turney, C.S.M., Allen, K., Fenwick, P., Cook, B.I., O'Donnell, A., Lough, J., Grierson, P., Baker, P., 2015. Drought variability in the eastern Australia and New Zealand summer drought atlas (ANZDA, CE 1500-2012) modulated by the Interdecadal Pacific Oscillation. Environ. Res. Lett. 10, 124002.
Patton, P.C., Pickup, G., Price, D.M., 1993. Holocene paleofloods of the Ross River, central Australia. Quat. Res. 40, 201–212.
Powell, D.M., 2009. Dryland rivers: processes and forms. In: Parsons, A.J., Abrahams, A.D. (Eds.), Geomorphology of Desert Environments. Springer, pp. 333–373.
Proske, U., Heslop, D., Haberle, S., 2014. A Holocene record of coastal landscape dynamics in the eastern Kimberley region, Australia. J. Quat. Sci. 29, 163–174.
Radke, L.C., Juggins, S., Halse, S.A., De, D.P., Finston, T., 2003. Chemical diversity in south-eastern Australian saline lakes II: biotic implications. Mar. Freshw. Res. 54, 895–912.
Ralph, T.J., Kobayashi, T., Garcia, A., Hesse, P.P., Yonge, D., Bleakley, N., Ingleton, T., 2011. Paleoecological responses to avulsion and floodplain evolution in a semiarid Australian freshwater wetland. Aust. J. Earth Sci. 58, 75–91.
Ramsay, H.A., Camargo, S.J., Kim, D., 2012. Cluster analysis of tropical cyclone tracks in the Southern Hemisphere. Clim. Dyn. 39, 897–917.
Reaney, S.M., 2008. The use of agent based modelling techniques in hydrology: determining the spatial and temporal origin of channel flow in semi-arid catchments. Earth Surf. Process. Landf. 33, 317–327.
Reeves, J.M., Bostock, H.C., Ayliffe, L.K., Barrows, T.T., Deckker, P.D., Devriendt, L.S., Dunbar, G.B., Drysdale, R.N., Fitzsimmons, K.E., Gagan, M.K., Griffiths, M.L., Haberle, S.G., Jansen, J.D., Krause, C., Lewis, S., McGregor, H.V., Mooney, S.D., Moss, P., Nanson, G.C., Purcell, A., van der Kaars, S., 2013a. Palaeoenvironmental change in tropical Australasia over the last 30,000 years—A synthesis by the OZ-INTIMATE group. Quat. Sci. Rev. 74, 97–114.
Reeves, J.M., Barrows, T.T., Cohen, T.J., Kiem, A.S., Bostock, H.C., Fitzsimmons, K.E., Jansen, J.D., Kemp, J., Krause, C., Petherick, L., Phipps, S.J., OZ-INTIMATE members, 2013b. Climate variability over the last 35,000 years recorded in marine and terrestrial archives in the Australian region: an OZ-INTIMATE compilation. Quat. Sci. Rev. 74, 21–34.
Risbey, J.S., Pook, M.J., McIntosh, P.C., Wheeler, M.C., Hendon, H.H., 2009. On the remote drivers of rainfall variability in Australia. Mon. Weather Rev. 137, 3233–3253.
Rouillard, A., Skrzypek, G., Dogramaci, S., Turney, C., Grierson, P.F., 2015. Impacts of high inter-annual variability of rainfall on a century of extreme hydrologic regime of northwest Australia. Hydrol. Earth Syst. Sci. 19, 2057–2078.
Sachs, J.P., Sachse, D., Smittenberg, R.H., Zhang, Z., Battisti, D.S., Golubic, S., 2009. Southward movement of the Pacific intertropical convergence zone AD 1400–1850. Nat. Geosci. 2, 519–525.
Schelske, C.L., Peplow, A., Brenner, M., Spencer, C.N., 1994. Low-background gamma counting: applications for ^{210}Pb dating of sediments. J. Paleolimnol. 10, 115–128.
Schidlowski, M., 1987. Application of stable carbon isotopes to early biochemical evolution on Earth. Annu. Rev. Earth Planet. Sci. 15, 47–72.
Schneider, T., Bischoff, T., Haug, G.H., 2014. Migrations and dynamics of the intertropical convergence zone. Nature 513, 45–53.
Shi, G., Ribbe, J., Cai, W., Cowan, T., 2008. An interpretation of Australian rainfall projections. Geophys. Res. Lett. 35, L02702.
Shook, K.R., Pomeroy, J.W., 2011. Memory effects of depressional storage in Northern Prairie hydrology. Hydrol. Process. 25, 3890–3898.
Shulmeister, J., 1992. A Holocene pollen record from lowland tropical Australia. The

Holocene 2, 107–116.
Shulmeister, J., Lees, B.G., 1995. Pollen evidence from tropical Australia for the onset of an ENSO-dominated climate at c. 4000 BP. The Holocene 5, 10–18.
Siebers, A.R., Pettit, N.E., Skrzypek, G., Fellman, J.B., Dogramaci, S., Grierson, P.F., in press. Alluvial ground water influences dissolved organic matter biogeochemistry of pools within intermittent dryland streams. Freshw. Biol. http://dx.doi.org/10.1111/fwb.12656.
Singarayer, J.S., Burrough, S.L., 2015. Interhemispheric dynamics of the African rainbelt during the late Quaternary. Quat. Sci. Rev. 124, 48–67.
Skrzypek, G., 2013. Normalization procedures and reference material selection in stable HCNOS isotope analyses: an overview. Anal. Bioanal. Chem. 405, 2815–2823.
Skrzypek, G., Dogramaci, S., Grierson, P.F., 2013. Geochemical and hydrological processes controlling groundwater salinity of a large inland wetland of northwest Australia. Chem. Geol. 357, 164–177.
Smith, M.A., Williams, A.N., Turney, C.S.M., Cupper, M.L., 2008. Human-environment interactions in Australian drylands: exploratory time-series analysis of archaeological records. The Holocene 18, 389–401.
Smith, M.A., Ross, J., 2008. What happened at 1500-1000 cal. BP in Central Australia? Timing, impact and archaeological signatures. The Holocene 18, 379–388.
Stager, J.C., Ryves, D.B., Chase, B.M., Pausata, F.S.R., 2011. Catastrophic drought in the Afro-Asian monsoon region during Heinrich event 1. Science 331, 1299–1302.
Stager, J.C., Ryves, D.B., King, C., Madson, J., Hazzard, M., Neumann, F.H., Maud, R., 2013. Late Holocene precipitation variability in the summer rainfall region of South Africa. Quat. Sci. Rev. 67, 105–120.
Stuut, J.-B.W., Temmesfeld, F., De Deckker, P., 2014. A 550 ka record of aeolian activity near North West Cape, Australia: inferences from grain-size distributions and bulk chemistry of SE Indian Ocean deep-sea sediments. Quat. Sci. Rev. 83, 83–94.
Sutfin, N.A., Shaw, J.R., Wohl, E.E., Cooper, D.J., 2014. A geomorphic classification of ephemeral channels in a mountainous, arid region, southwestern Arizona, USA. Geomorphology 221, 164–175.
Taschetto, A.S., England, M.H., 2009. An analysis of late twentieth century trends in Australian rainfall. Int. J. Climatol. 29, 791–807.
Tierney, J.E., Oppo, D.W., Rosenthal, Y., Russell, J.M., Linsley, B.K., 2010. Coordinated hydrological regimes in the Indo-Pacific region during the past two millennia. Paleoceanography 25, PA1102.
Tierney, J.E., Smerdon, J.E., Anchukaitis, K.J., Seager, R., 2013. Multidecadal variability in East African hydroclimate controlled by the Indian Ocean. Nature 493, 389–392.
van der Kaars, S., De Deckker, P., 2002. A Late Quaternary pollen record from deep-sea core Fr10/95, GC17 offshore Cape Range Peninsula, northwestern Western Australia. Rev. Palaeobot. Palynol. 120, 17–39.
van der Kaars, S., De Deckker, P., Gingele, F.X., 2006. A 100 000-year record of annual and seasonal rainfall and temperature for north-western Australia based on a pollen record obtained offshore. J. Quat. Sci. 21, 879–889.
van Etten, E.J.B., 2009. Inter-annual rainfall variability of arid Australia: greater than elsewhere? Aust. Geogr. 40, 109–120.
Verschuren, D., 1999. Sedimentation controls on the preservation and time resolution of climate-proxy records from shallow fluctuating lakes. Quat. Sci. Rev. 18, 821–837.
Verschuren, D., 2004. Decadal and century-scale climate variability in tropical Africa during the past 2000 years. In: Battarbee, R.W., Gasse, F., Stickley, C.E. (Eds.), Past Climate Variability through Europe and Africa, vol. 6. Springer, Dordrecht, pp. 139–158.
Verschuren, D., Charman, D.J., 2008. Latitudinal linkages in late Holocene moisture-balance variation. In: Battarbee, R.W., Binney, H.A. (Eds.), Natural Climate Variability and Global Warming: a Holocene Perspective. Wiley-Blackwell, Chichester, UK, pp. 189–231.
Villalba, R., Lara, A., Masiokas, M.H., Urrutia, R., Luckman, B.H., Marshall, G.J., Mundo, I.A., Christie, D.A., Cook, E.R., Neukom, R., others, 2012. Unusual Southern Hemisphere tree growth patterns induced by changes in the Southern Annular Mode. Nat. Geosci. 5, 793–798.
Western Mail, 1917. Our Flocks and Herds, 21 December 1917. Edition: CHRISTMAS. Trove (Perth, WA : 1885–1954). Available from: http://nla.gov.au/nla.news-article37443627 (20 August 2014).
Williams, A.N., 2013. A new population curve for prehistoric Australia. Proc. R. Soc. B Biol. Sci. 280, 389–401.
Williams, A.N., Veth, P., Steffen, W., Ulm, S., Turney, C.S.M., Reeves, J.M., Phipps, S.J., Smith, M., 2015. A continental narrative: human settlement patterns and Australian climate change over the last 35,000 years. Quat. Sci. Rev. 123, 91–112.
Woodborne, S., Hall, G., Robertson, I., Patrut, A., Rouault, M., Loader, N.J., Hofmeyr, M., 2015. A 1000-year carbon isotope rainfall proxy record from South African baobab trees (*Adansonia digitata* L.). PLoS One 10, e0124202.
Yan, H., Sun, L., Wang, Y., Huang, W., Qiu, S., Yang, C., 2011. A record of the Southern Oscillation Index for the past 2,000 years from precipitation proxies. Nat. Geosci. 4, 611–614.
Yan, H., Wei, W., Soon, W., An, Z., Zhou, W., Liu, Z., Wang, Y., Carter, R.M., 2015. Dynamics of the intertropical convergence zone over the western Pacific during the Little Ice Age. Nat. Geosci. 8, 315–320.
Yancheva, G., Nowaczyk, N.R., Mingram, J., Dulski, P., Schettler, G., Negendank, J.F.W., Liu, J., Sigman, D.M., Peterson, L.C., Haug, G.H., 2007. Influence of the intertropical convergence zone on the East Asian monsoon. Nature 445, 74–77.